Sustainable Materials and Technologies 49 (2026) e02136

Contents lists available at ScienceDirect

Sustainable Materials and Technologies

journal homepage: www.elsevier.com/locate/susmat

Complete metal recovery from tantalum capacitors via hydrometallurgy

Flavia N. Braga [a,b], Maria C. Hespanhol [c,*], Ana M. Ferreira [a], Ana C.R.V. Dias [d], Helena Passos [b], Nicolas Schaeffer [a], João A.P. Coutinho [a]

[a] CICECO - Aveiro Institute of Materials, Department of Chemistry, University of Aveiro, 3810-193 Aveiro, Portugal
[b] LSRE-LCM, ALiCE, Faculty of Engineering, University of Porto, Rua Dr. Roberto Frias, 4200-465 Porto, Portugal
[c] Group of Analysis and Education for Sustainability (GAES), Chemistry Department, Federal University of Viçosa (UFV), Viçosa 36570-900, Minas Gerais, Brazil
[d] CESAM – Centre for Environmental and Marine Studies, Department of Environment and Planning, University of Aveiro, 3810-193 Aveiro, Portugal

ARTICLE INFO

Keywords:
Tantalum capacitors
Hydrometallurgy
Metal recovery
Selective leaching
Solvent extraction
Circular economy

ABSTRACT

The rapid advancement of technology and the shortened lifespan of electronic devices have intensified the global e-waste crisis, leading to a growing accumulation of waste tantalum capacitors (TC). Due to their high capacitance and reliability, TC are widely used from smartphones to aerospace systems. Ta, the key component in waste TC, is classified as a critical raw material by the European Union; yet less than 1% is recovered from end-of-life devices. This study proposes a complete hydrometallurgical flowsheet that looks beyond conventional Ta-centric approaches to the recovery of all metallic constituents from TC. The process intentionally retains Ta in the solid phase as Ta_2O_5, eliminating energy-intensive reduction steps and allowing its direct reuse in industrial applications. Optimized sulfuric-acid leaching selectively dissolves Mn, Ni, Cu, and Zn, while retaining Ta and Ag in the solid residue. The leachate undergoes Mn precipitation and sequential solvent extraction with CYANEX® 272, yielding metal salts with industrially relevant purities (93% Zn; 98% Cu and Ni) and high overall recoveries (91% Zn; 91% Cu; 84% Ni). Subsequent nitric acid leaching dissolves Ag, later precipitated via chloride addition, leaving Ta in the solid fraction with 85% purity. Life-cycle assessment results show substantial impact reduction across all categories compared to primary production, with Ta and Ag recovery as the main contributors to sustainability gains. A preliminary cost analysis further confirms the economic viability of the process. These findings demonstrate its potential as a sustainable route for recovering critical and valuable metals while advancing circular-economy in the electronics sector.

1. Introduction

The rapid development of technology and the growing demand for electronic devices have led to a significant increase in the Waste Electrical and Electronic Equipment (WEEE), commonly known as e-waste, worldwide. As consumers upgrade to newer gadgets and manufacturers release innovative products at an unprecedented pace, discarded electronics have become the fastest-growing waste stream. The Global *E*-Waste Monitor reports that annual e-waste generation increased from 34 Mt. in 2010 to 62 Mt. in 2022, and projections indicate this trend will continue to rise to 82 Mt. by 2030 [1].

Capacitors, essential components of electronic circuits, significantly contribute to the e-waste generated annually [2]. The global capacitor market was valued at USD 38.91 billion in 2024 and is projected to exceed USD 69.42 billion by 2034 [3]. These passive electrical devices feature two terminals that enable energy storage within an electric field, playing a critical role in the functionality of modern electronics [4]. Tantalum capacitors (TC) stand out among the various types of capacitors due to their exceptional volumetric efficiency, which enables highly compact designs while delivering outstanding performance [5–7]. The main components that constitute TC are Ta, Si, Mn, Fe, Ni, Cu, Ag, and Sn [2]. In these devices, Ta accounts for 30–50% [8,9] and is the most valuable metal due to its superior characteristics, which suit most high-tech applications. Ta is valued for its unique combination of properties, including exceptional acid corrosion resistance, high ductility, superior wear resistance, biocompatibility, high melting point, excellent strength at elevated temperatures, and the ability to efficiently store and release electrical charge. These attributes make it the material of choice for a wide range of specialized applications across industries, including automotive, aerospace, chemical processing, defense, electronics, medical devices, and metallurgy [10,11].

The recognition of tantalum as a critical raw material by the

* Corresponding author.
E-mail address: mariacarmo@ufv.br (M.C. Hespanhol).

https://doi.org/10.1016/j.susmat.2026.e02136
Received 3 March 2026; Received in revised form 8 June 2026; Accepted 24 June 2026
Available online 28 June 2026

European Union [12] highlights growing concerns regarding its secure supply. This classification is primarily driven by the limited geographical availability of primary resources and the socio-environmental risks associated with its extraction, which is largely concentrated in the Great Lakes region of Africa. There, production is dominated by artisanal and small-scale mining, frequently linked to inadequate labor conditions, regulatory instability, and conflict financing [13]. These factors not only compromise supply chain transparency but also expose global markets to price volatility and geopolitical risks, reinforcing the urgency of developing alternative sourcing strategies.

The use of Ta in capacitors accounts for 34% of the annual demand [5] but the recycling rate of this metal from current end-of-life products is still less than 1% [6]. In response to this low rate, several recovery strategies were developed to specifically address waste tantalum capacitors (WTC). The recycling chain of WTC begins with the identification, disassembling, and crushing of the devices, followed by extraction and refining to enhance the purity of the recovered Ta. Further pre-treatment steps can be applied to isolate Ta from contaminants, such as thermal, physical, and mechanical treatments. Thermal treatments typically involve the application of high temperatures or the combustion of TC to extract the metal. On the other hand, physical or mechanical separation processes rely on the distinct physical properties of the constituent materials, such as density, weight, or size, to achieve separation and recovery [2].

Although WTC contain several valuable metals, such as Mn, Ni, Cu, Ag, Fe and Zn, most reported recovery processes remain heavily focused on Ta. Most studies and patents aim at obtaining either tantalum oxide or high-purity metallic Ta, often through chloride metallurgy [14–16], magnesiothermal reduction [17,18], electron beam melting [18,19], high-temperature roasting [20,21], or solvent-based hydrometallurgy [14,19,22–27]. In these approaches, coexisting metals are either removed as impurities, lost during leaching, or entirely disregarded. Even when other metals are partially recovered [8,13,28], processes are still optimized primarily for the extraction and purification of Ta. This systematic neglect of secondary metals limits the sustainability of existing approaches and underscores the need for more integrated flowsheets that valorize the full metal content of WTCs.

The most reported method for extracting Ta is hydrometallurgy. Within this approach, Ta extraction typically relies on aggressive chemical media, particularly hydrofluoric acid (HF) [23]. While highly effective for Ta extraction, HF-based leaching presents several issues due to its corrosivity, its volatility that can lead to atmospheric pollution, and the process produces fluorine-containing wastewater and solid residues, posing significant environmental risks [29]. Furthermore, in HF-based hydrometallurgical extraction, Ta is recovered in the form of complex compounds or soluble species, which require further conversion steps—such as precipitation, roasting, or reduction—to obtain Ta in its usable metallic or oxide form [23]. These additional transformations contribute to increased process complexity, cost, and energy demand. Although alternative systems based on highly concentrated alkaline solutions, such as potassium hydroxide (KOH), were proposed as less hazardous substitutes for Ta dissolution, they generally exhibit lower extraction efficiencies (~70%) [27].

To mitigate these issues, alternative hydrometallurgical strategies were explored to employ milder leaching agents that selectively dissolve base and transition metals, while retaining Ta in the solid residue [2]. Agrawal et al. [28] applied a leaching step using HCl to extract Mn and Ni, while Xia et al. [8] combined cryogenic grinding, alkaline calcination and HNO_3 leaching to solubilize Fe, Ni, and Ag. Niu et al. [16] applied magnetics separation to recover Ni—Fe terminals and chloride metallurgy to isolate Ta in the solid. Although these strategies demonstrate promising steps toward Ta recovery, none of them achieve the full recovery of all valuable metals present in TC. Within this context, an underexplored opportunity lies in the use of H_2SO_4, which is widely applied in the mineral ore industry [30,31] but has not yet been explored for TC recovery. Compared to HCl, H_2SO_4 offers several advantages: it is significantly less volatile, sulphate ions are generally less corrosive and less disruptive to downstream processes than chloride ions, and it is often more cost-effective.

In this study, we propose a novel hydrometallurgical strategy that departs from the Ta-centric approach commonly found in literature. By employing a two-step leaching process using H_2SO_4 followed by HNO_3, our method enables the selective dissolution and recovery of multiple metals with industrially relevant purities, namely Mn, Ni, Cu, Zn, and Ag, while intentionally retaining Ta in the solid phase. Unlike conventional approaches that prioritize Ta and treat other metals as secondary or incidental, our method is conceived from the outset as a complete recovery platform. The resulting Ta-rich residue corresponds directly to Ta_2O_5, which can be readily used in industrial applications. Meanwhile, the coexisting metals are recovered in sulfuric solutions that are compatible with downstream processing. This approach eliminates unnecessary purification steps for Ta recovery, thereby enhancing the overall sustainability and practicality of WTC valorization.

2. Materials and methods

2.1. Materials

Tantalum capacitors were purchased from the Chinese Super Electronic Market via Aliexpress. The TC used in this study were SMD-type components with 470 μF/6.3 V nominal ratings and 7343 (EIA D-case) encapsulation, corresponding to dimensions of 7.3 × 4.3 mm. A scheme of the capacitor is present in Fig. 1a. Hydrochloric acid (37 wt%) was purchased from Honeywell. Nitric acid (65 wt%) and potassium permanganate (99 wt%) were acquired from Merck. Yttrium standard (983 $mg{\cdot}kg^{-1}$ of Y(III) in 2% nitric acid), Triton® X-100, poly(vinyl alcohol) (87–90 wt%), dodecane (99 wt%) and ammonia solution (28–30 wt%) were purchased from Sigma-Aldrich. SERVA was the supplier of silicone solution SERVA in isopropanol. Sodium chloride (extra pure) was acquired from LabKem, sulfuric acid (95%) from Fisher Chemical, and CYANEX® 272 (bis(2,4,4-trimethylpentyl)phosphinic acid – 90 wt%) from BLDpharm. All chemicals were used as received without further purification.

2.2. Sample preparation and characterization

New TC were obtained and carefully cracked open using a bench vice (Fig. 1b). The material in the interior was subsequently ground into finer particles using a Fritsch Pulverisette 23 ball mill, equipped with a zirconium oxide chamber and five zirconium oxide grinding balls. The milling process was carried out at a frequency of 50 s^{-1} for a total duration of 60 min, with alternating cycles of 10 min of operation followed by a 3 min pause.

The characterization of the TC was conducted using different analytical techniques. The solid in powder form was analyzed using both scanning electron microscopy with energy dispersive spectroscopy (SEM-EDS), conducted with a Bruker Nano GmbH microscope, and X-ray diffraction (XRD), using a Bruker AXS instrument with Cu Kα radiation at 45 kV. The XRD diffractograms were analyzed with the X'pert Highscore Plus software package, and the resulting patterns were compared to the International Center for Diffraction Data (ICDD) database for identification. The particle size distribution of the milled TC powder was measured by laser diffraction using a Coulter LS 230 Particle Size Analyzer. Measurements were performed in duplicates, and the results were expressed as d10, d50, and d90 particle diameters.

2.3. Metal quantification

Metal quantification was performed using Total Reflection X-ray Fluorescence (TXRF) spectrometry, specifically the Picofox S2 model (Bruker Nano), which features a molybdenum X-ray source. The measurements were conducted under operating conditions of 50 kV voltage

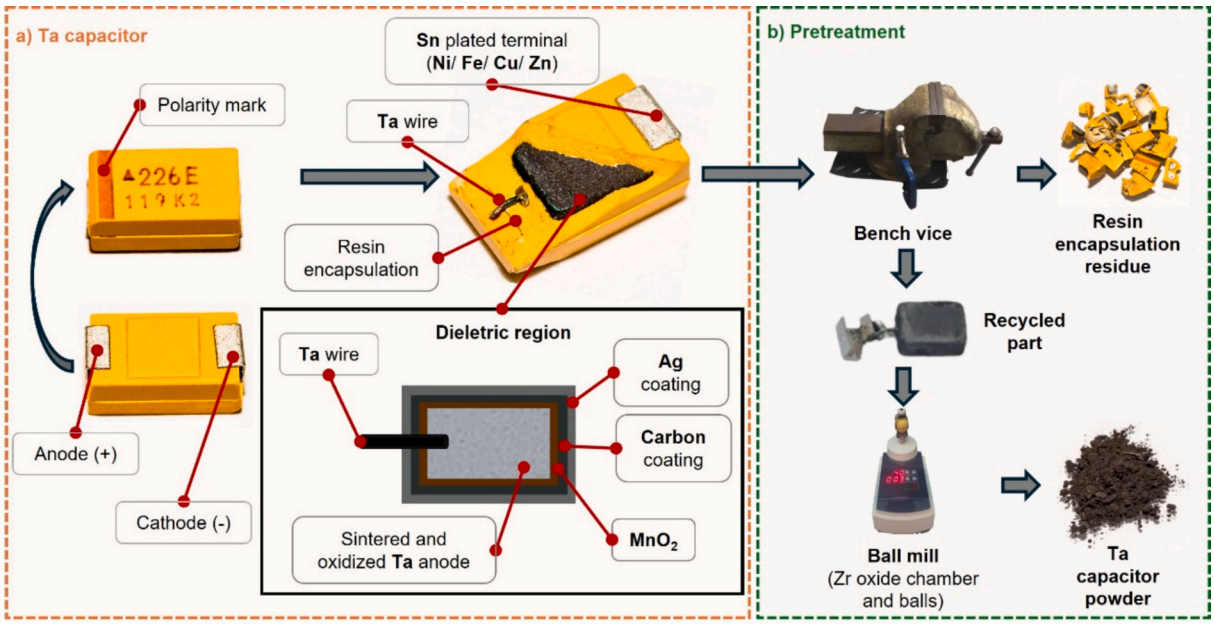

Fig. 1. Structure and pretreatment of solid Ta capacitors: a) internal components and construction; b) pretreatment steps for resin removal and powder preparation.

and 600 μA current. Quartz glass carriers were pre-coated with 10 μL of a silicon-in-isopropanol solution (SERVA) and dried at 323 K. The liquid samples were prepared by diluting them in a 1 wt% polyvinyl alcohol in 2% nitric acid solution and spiked with a known concentration of an yttrium standard, tailored to the metal content of the samples. The solid samples were prepared by adding 1 wt% Triton® X-100 to facilitate the formation of a stable suspension. TXRF analysis of solid residues was used only for qualitative monitoring of the persistence of elements such as Sn and Zr in the solid phase throughout the process. In both cases, a 10 μL aliquot of the prepared solution was deposited onto the pre-treated quartz carrier and dried at 353 K prior to analysis. Analyses were performed for 240 s of exposure of each quartz carrier. The results are expressed in milligrams of metal per kilogram of solution.

2.4. Leaching

Leaching experiments were performed using a Radleys Tech Carousel apparatus, unless otherwise specified, with temperature regulation provided by a circulating water bath and constant agitation maintained at 600 rpm. The initial conditions evaluated focused on the type of acid used, specifically 2 M HNO_3, 2 M H_2SO_4, and 2 M HCl for 2 h. The leaching extraction (LE) of metals is represented in the form of grams of metal leached per 100 g of TC powder as calculated by Eq. (1):

$$\mathrm{LE}\left(\frac{\mathrm{g}}{100\ \mathrm{g}}\right) = \mathrm{C_m}\left(\frac{\mathrm{g}}{\mathrm{kg}}\right) \times \frac{\mathrm{m_{ls}\ (kg)}}{\mathrm{m_{TC}\ (g)}} \times 100 \quad (1)$$

where C_m is the concentration of metal obtained in TXRF, m_{ls} is the mass of leaching solution and m_{TC} is the mass of TC used in the leaching process.

The representation of the leaching results as grams of metal leached per 100 g of TC rather than as extraction percentages was selected because the total metal inventory of the feed material was not determined by complete digestion. Accurate quantification of the absolute metal content would require HF-based digestion of the Ta-containing phases, which was not pursued due to the associated safety concerns and because it was not essential for the objectives of this study. Therefore, this metric provides a direct measure of metal dissolution based exclusively on experimentally determined leachate concentrations.

To explore potential synergies or antagonisms in the extraction process under varying conditions, response surface methodology (RSM, see section 2.5.) was used. After determining the optimal conditions for the best-performing acid (H_2SO_4), a kinetic study was conducted to ascertain the time required for the leaching of Mn, Ni, Cu, and Zn and to understand the mechanisms of metal extraction. The optimized leaching process was then conducted in a round-bottom flask immersed in a temperature-controlled paraffin bath. This setup facilitated the production of a substantial volume of leaching solution, enabling further exploration of subsequent steps.

Following the leaching process, the mixture was subjected to centrifugation in a Falcon tube for 40 min at 6000 rpm using a NEYA 16R centrifuge (REMI), with an acceleration time of 1 min and a deceleration time of 1 min. Subsequently, the phases were separated. The solid phase was washed three times with the leaching solution and dried overnight at 50 °C in an oven to prepare for TXRF analysis. Meanwhile, the liquid phase was diluted and analyzed by TXRF.

2.5. Optimization using RSM

Response Surface Methodology (RSM) combines mathematical and statistical techniques to model relationships between experimental variables and responses, facilitating process understanding and optimization [32]. In this approach, a response (y) is typically described by a second-order polynomial model, as expressed in Eq. (2):

$$y = \beta_0 + \sum \beta_i X_i + \sum \beta_{ii} X_i^2 + \sum_{i<j} \beta_{ij} X_i X_j \quad (2)$$

where, β_0, β_i, β_{ii}, and β_{ij} are the regression coefficients for the intercept, linear, quadratic, and interaction terms, respectively, and X_i and X_j represent the coded levels of the independent variables.

In factorial experimental designs, a 2^k design explores all possible combinations of k variables at two levels (typically coded as −1 and + 1), allowing the estimation of main effects and two-way interactions. When complemented with axial points and center-point replicates, it forms a central composite rotatable design (CCRD), which supports the fitting of quadratic models within the RSM framework.

In this study, two RSM-based CCRDs were implemented. The first design was a 2^3 CCRD, applied to optimize the leaching of Mn, Ni, Cu, and Zn with H_2SO_4, while minimizing the co-extraction of Ta and Ag. The independent variables were temperature (61–95 °C), H_2SO_4 concentration (0.5–3.5 M), and solid-to-liquid ratio (1/101 to 1/11 *w*/w),

with a fixed contact time of 2 h. A total of 20 experiments were conducted as detailed in Tables S1 and S2 (Supplementary Material).

The second design followed a 2^2 CCRD, focused on the subsequent leaching of the solid residue using HNO_3, with the goal of maximizing Ag recovery and minimizing Ta extraction. The variables studied were HNO_3 concentration (0.6–3.4 M) and temperature (49–95 °C), while the S/L ratio (1/10 *w*/w) and contact time (2 h) were kept constant. A total of 11 experiments were performed, as detailed in Tables S3 and S4 (Supplementary Material).

All statistical analyses were performed using *Statistica* 10.0 software (StatSoft Inc., Tulsa, OK, USA), with a 95% confidence level. Model adequacy was assessed by analysis of variance (ANOVA), regression coefficients (R^2), and lack-of-fit tests. Response surface and contour plots were used to visualize variable interactions and to identify the optimal leaching conditions in this study.

2.6. Metal separation

After leaching with sulfuric acid under optimized conditions, the obtained leachate was subjected to a series of procedures to separate the remaining metals. The first target was Mn, which was selectively removed by adding potassium permanganate ($KMnO_4$) in the stoichiometric ratio defined by the overall reaction ($3Mn^{2+} + 2MnO_4^- \rightleftharpoons 5MnO_2 + 4H^+$). This addition prompted the precipitation of Mn. The solid was separated from the liquid phase by centrifugation (30 min at 7000 rpm). The liquid phase was analyzed in TXRF.

The subsequent steps involved metal extraction using a 0.4 M solution of CYANEX® 272 in n-dodecane, a concentration previously reported to be sufficient for achieving complete extraction of the target metals from sulfuric media [33]. A range of pH values, from the original 0.2 to 8.5, was tested to determine the optimal conditions for extracting each metal. The pH was adjusted using ammonia to ensure the formation of stable complexes of Zn and Cu in the respective extraction pHs [34], and was measured with a SevenExcellence pH meter (Mettler Toledo).

Each extraction experiment was conducted individually in 2 mL Eppendorf tubes at room temperature, maintaining a 1:1 *w*/w between the leachate and the organic mixture. The phase ratios were controlled using an analytical balance. All extraction experiments were performed in duplicate, and each sample was analyzed twice. The contact time for each test was set to 30 min, which was deemed sufficient to achieve equilibrium between the aqueous and organic phases. This duration was based on prior studies demonstrating that equilibrium could be attained in similar systems within 5 min [35]. After that, the vials were centrifuged (5 min at 3000 rpm) and the aqueous and organic phases were separated. The aqueous phases were analyzed by TXRF. The metals were stripped from the organic phases using H_2SO_4 at different concentrations (0.01, 0.05, 0.1, 0.5, 1, and 2 M).

Metal purities in each phase were determined based on TXRF analysis. The phase containing the extracted metal was analyzed, and the masses of all detected metals were quantified. The purity of the target metal was subsequently calculated by dividing its mass by the total mass of metals present in that phase.

Regarding the second leaching step, following dissolution with HNO_3 under optimized conditions, the resulting leachate was submitted to a precipitation process by the addition of NaCl, resulting in a final salt concentration of 3 wt%.

2.7. Life cycle assessment

A life cycle assessment (LCA) was performed to evaluate the environmental impacts of the innovative hydrometallurgical process proposed in this study for metal recovery from TC, following the guidelines established by the ISO 14040 [36] and ISO 14044 [37] standards. The system boundaries include the proposed process, as well as the production of all inputs (chemicals, water, and electricity). The functional unit was the processing of 1 kg of TC.

The inventory data regarding the inputs and outputs from the process are presented in Table S5 (Supplementary Material). Data on chemical and water consumption were derived from the laboratory-scale experiments. CYANEX® 272 and dodecane were assumed to be reused with an estimated loss of 5% [38]. Accordingly, only the make-up quantities required to compensate for these losses were considered as inputs in the life cycle inventory. Electricity is consumed in several process operations, including milling, heating, mixing and filtration. Given that laboratory-scale electricity consumption typically overestimates industrial-scale values, electricity consumption was estimated based on thermodynamic calculations for heating, while literature data were used for the remaining operations. For milling, a consumption of 0.01 kWh/kg of material was adopted [39]. For mixing, the power was estimated based on the type of mixture (2 kW/L for slurry suspension, 0.1 kW/L for simple mixing, 1.5 kW/L for liquid-liquid mixing) and the volume, combined with the duration of the operation [40]. For filtration, a consumption of 0.005 kWh/L of filtrate was considered [41]. Data on the production of the inputs were sourced from the ecoinvent database version 3.11 [42]. The impact assessment was conducted using the Environmental Footprint 3.1 method [43] as recommended by the European Commission.

3. Results and discussion

3.1. Leaching

To develop an efficient process for Ta recovery from TC, it is essential to first understand the structure and composition of the material. The standard architecture of the SMD TC used includes a porous Ta anode, a Ta_2O_5 dielectric layer, and a MnO_2 cathode (Fig. 1a). Conductive coatings usually comprise graphite and Ag, while the external terminals are commonly coated with Sn and may include underlying layers of Cu, Zn, Ni, and/or Fe, depending on the specific metallization used by the manufacturer [6,17]. This configuration was validated by the characterization results, which revealed the elemental composition and distribution within the capacitor, as shown in Fig. 2 and Fig. S1. Prior to leaching, the capacitors were milled and the particle size distribution of the resulting powder was determined by laser diffraction. The milled powder exhibited a mean particle size of 20.1 μm, with d10, d50, and d90 values of 2.56, 13.95, and 48.47 μm, respectively.

As illustrated in Fig. 2c-d, Ta and Mn are the dominant components in the solid fraction. This aligns with their structural roles as the anode and cathodic layers, further supported by the EDS mapping (Fig. 2a-b and Fig. S1). The XRD analysis (Fig. 2d) confirms the presence of Ta_2O_5 and MnO_2 phases, although the tantalum peaks suggest a potential mixture of metallic and oxidized forms. Sn and Ag were also detected - Sn originating from external solder contacts, and Ag from conductive pastes or terminations, as evidenced by its spatial distribution near the Mn-rich layer (Fig. 2b). Zr, which is not typically found in TC components [2], is attributed to contamination introduced during the milling process, likely from abrasion of ZrO_2-based components of the ball mill. Although its detected amount is non-negligible, this impurity was not further considered in the process assessment, as improved selection of milling materials should readily eliminate this source of contamination. Moreover, Zr remains confined to the solid residue and does not interfere with the leaching or subsequent separation steps.

Zn can be identified in the plated terminal but other metals such as Ni and Cu are present in the solid in lower concentrations, below the EDS detection threshold in the powder, and can only be reliably quantified after leaching, when their concentration in solution becomes detectable by TXRF (Fig. 2e). Considering the presence of these elements, three inorganic acids – HNO_3, H_2SO_4, and HCl – were initially evaluated for their leaching performance at a concentration of 2 M. These acids were selected based on their known effectiveness in dissolving a wide range of metals commonly found in electronic waste, their industrial maturity,

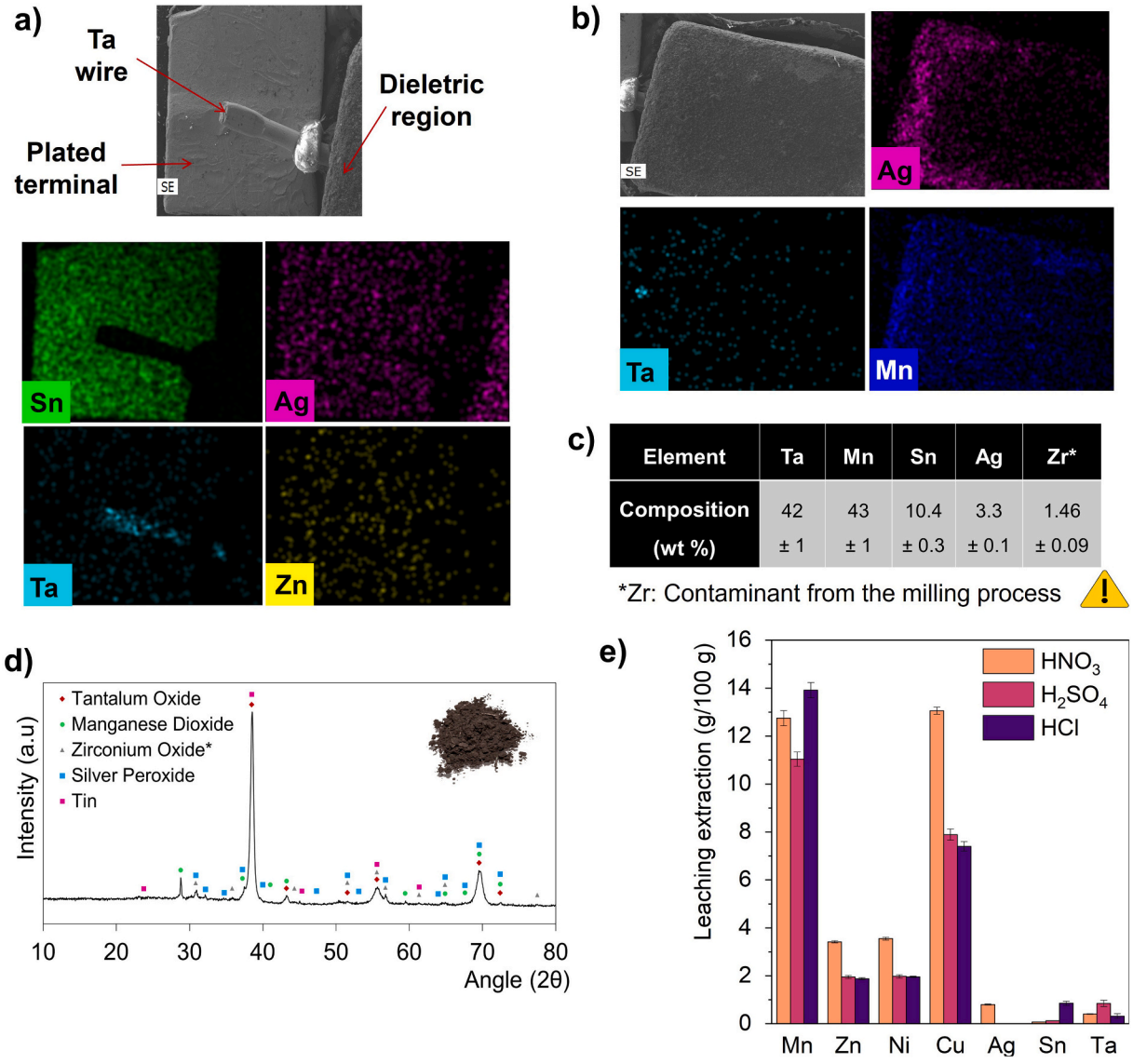

Fig. 2. Characterization of TC: SEM-EDS elemental mapping of (a) the plated terminal with the Ta wire and of (b) the dielectric region, showing the distribution of Sn (green), Ta (blue), Mn (dark-blue) and Ag (pink); (c) Elemental composition of the TC powder determined by SEM–EDS (wt%); (d) XRD diffractogram of the powdered TC sample, identifying crystalline phases; (e) metal leaching extraction from TC using different acids ([acid] = 2 M, S/L ratio = 1/100, $T = 95$ °C, $t = 2$ h). *Zr is an inert contaminant from the milling process.

and affordability [22,24,27,30,31,44]. The results are shown in Fig. 2e. The leaching efficiencies observed are closely related to the redox potential of the target metals relative to the leaching system, as well as to the solubility of the compounds formed. For reference, the standard electrode potential (E^0) for the elements/compounds of interest is presented in Table S6 [45].

Zn and Ni, with standard potentials of −0.762 and − 0.257 V, respectively (both lower than that of the H^+/H_2 couple) undergo spontaneous oxidation in acidic media, which explains their consistent dissolution across all tested acids. Cu, with a higher potential of +0.342 V, is harder to extract and necessarily requires an auxiliary oxidant: dissolved oxygen in H_2SO_4 and HCl enables moderate extraction, while HNO_3 achieves higher extraction of Cu, as well as Zn and Ni, due to the strong oxidizing capacity of nitrate ions.

Ag, with an even higher reduction potential of +0.8 V, is not dissolved in H_2SO_4, partly because any Ag^+ formed has a limited solubility in sulfate media and Ag_2SO_4 tends to precipitate and thereby restrict further dissolution [46]. The formation of Ag_2SO_4 was later confirmed with the XRD analysis of the solid after H_2SO_4 leaching (Fig. S14). When nitric acid is used, the strongly oxidizing nitrate ion enables the effective oxidation and dissolution of Ag, in addition to the metals already leached by H_2SO_4.

Mn is present as MnO_2, which dissolution requires reduction to Mn^{2+} (Table S6). HCl provides slightly higher Mn extraction, likely due to chloride-assisted redox reactions and complexation that facilitate MnO_2 reduction, producing soluble Mn-chloride species [47].

$$(MnO_{2(s)} + 4HCl_{(aq)} \rightleftharpoons MnCl_{2(aq)} + 2H_2O_{(l)} + Cl_{2(g)})$$

Ta remains in the solid phase under the investigated leaching conditions due to its exceptional chemical inertness. Metallic Ta rapidly forms a nanometric Ta_2O_5 passivation layer when exposed to oxygenated or aqueous environments, which is highly stable and insoluble in common mineral acids (H_2SO_4, HCl, HNO_3) [48,49]. Industrial and laboratory studies have consistently shown that efficient Ta dissolution requires fluoride-based media, typically concentrated hydrofluoric acid (40–48%) or HF– H_2SO_4 mixtures, which form stable fluor-complexes [50].

The potential of H_2O_2 as an oxidizing agent in H_2SO_4 leaching was also evaluated; however, no significant improvement in metal extraction

was observed for Mn, Ni, Cu, and Zn, while the undesired Ta dissolution increased (Fig. S2). As a result, its implementation was not carried out.

Based on these observations, a two-step leaching strategy can be proposed – Fig. 3. The first step involves using H_2SO_4 to the selective leaching of Mn, Ni, Cu, and Zn, while retaining Ag and Ta in the solid phase. The dissolution of the base-metal-containing phases during this stage can be generally represented by Eq. (3):

$$MO + H_2SO_4 \rightleftharpoons MSO_4 + H_2O \quad (3)$$

where M represents Mn, Ni, Cu, or Zn. The second step uses HNO_3 to dissolve Ag from the remaining solid of the first leaching stage, leaving Ta in the solid phase. The dissolution of Ag in dilute nitric acid can be generally represented by Eq. (4):

$$3Ag + 4HNO_3 \rightleftharpoons 3AgNO_3 + NO + 2H_2O \quad (4)$$

Although both HCl and H_2SO_4 show similar inefficiency toward Ag and Ta extraction, H_2SO_4 was selected as the leaching agent in the first step due to its operational and environmental advantages. It is considerably less volatile and less corrosive to common process equipment, reducing safety concerns and material degradation. Unlike HCl, it does not release chlorine-containing gaseous emissions such as Cl_2 or HCl vapors, simplifying gas treatment and minimizing environmental impact. Furthermore, H_2SO_4 is a lower-cost and more widely available reagent, making it the preferred option for scaling up the process [51].

3.1.1. 1st (H_2SO_4) leaching step optimization

Response Surface Methodology was applied to optimize the leaching step with H_2SO_4, allowing the identification of the most significant variables and their interactions. The independent variables considered were temperature (61–95 °C), H_2SO_4 concentration (0.5–3.5 M), and solid-to-liquid ratio (S/L, 1/101 to 1/11 *w*/w). The response variables were the extraction yields of Mn, Ni, Cu, and Zn (to be maximized), and Ta and Ag (to be minimized). All experiments were performed with a fixed contact time of 2 h. The detailed results are presented in the Supplementary Material (Tables S7–S17, Figs. S3-S12). Model fitting was evaluated using analysis of variance (ANOVA), with all models demonstrating good predictive accuracy, as evidenced by coefficients of determination (R^2) ranging from 0.85 to 0.93 and F-calculated > F-tabulated, confirming the reliability of the models in describing the experimental data. In all cases, the interpretation of the effects of the operational variables was based on the response surface analysis, which accounts simultaneously for the linear, quadratic, and interaction terms of the fitted models. The influence of the independent variables on metal extraction is illustrated in Fig. 4, which presents response surface plots for Mn, Zn, and Ta; the corresponding plots for Ni and Cu, which exhibited similar trends to Mn, are provided in the Supplementary Material (Fig. S13) to improve clarity and avoid redundancy. Note that Ag was not detected under any of the experimental conditions evaluated.

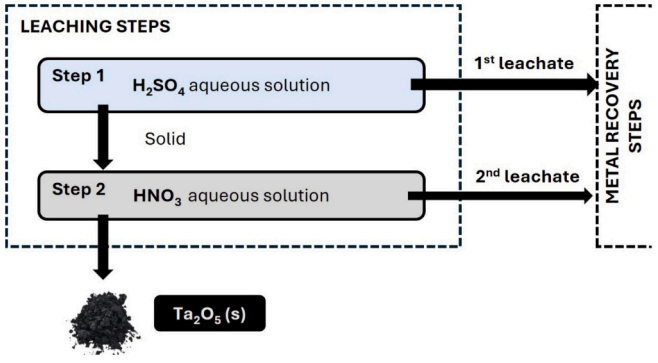

Fig. 3. Schematic representation of the proposed two-step leaching process using H_2SO_4 and HNO_3 for metals recovery from TC. The dissolved metals are processed in subsequent metal recovery steps.

The influence of the operational variables on metal extraction is illustrated in the response surface plots (Fig. 4 and Fig. S13) and corroborated by the Pareto charts (Figs. S3, S5, S7, S9, and S11, Supplementary Material).

From the analysis, Mn, Ni, Cu and Zn had a similar behavior: S/L ratio and temperature had a significant effect, and the quadratic effects of all three variables (S/L ratio, temperature, and acid concentration) were also significant and negative, indicating the presence of optimal values beyond which extraction efficiency declined, consistent with the appearance of maxima in the response surfaces.

In the case of Ta, the most critical effect was observed for the interaction between temperature and S/L ratio, followed by the individual effects of acid concentration, temperature, and S/L ratio. However, the observed trends were opposite to those of the other metals: higher temperature and S/L ratio had a negative effect on Ta extraction, while acid concentration had a positive effect, i.e., higher acid concentrations promoted increased Ta dissolution. These distinct trends highlight the different extraction mechanisms involved and guide the selection of leaching conditions.

Since the objective was to maximize the extraction of Mn, Ni, Cu, and Zn while minimizing Ta solubilization, response surface analysis indicated that optimal extraction occurs within a region defined by high temperatures (85–95 °C), elevated S/L (0.09–0.11 g/mL), and moderate H_2SO_4 concentrations (0.9–1.5 M). Based on this, the optimal conditions were defined as 90 °C, 1.4 M acid concentration, and a solid-to-liquid ratio of 1/10 (*w*/w). Under optimal conditions, the experimental leaching extraction of metals values are presented in Table 1 and showed good agreement with the model predictions, with relative errors below 14%. Ta extraction remained very low (0.032 ± 0.005) g/100 g, and Ag was not detected.

The residual solid obtained after H_2SO_4 leaching was characterized by SEM-EDS (Table S18, Fig. S14) and XRD (Fig. S15). Overall, the compositional changes observed in the EDS mapping (Fig. S14) and quantification (Table S18) confirm that H_2SO_4 effectively dissolves Mn-based and other soluble components, while Ta and Ag are largely undissolved. The XRD pattern supports these findings, with Ta as the dominant phase. The coexistence of silver oxide and sulfate indicates that part of the silver as leached and reprecipitated as poorly soluble Ag_2SO_4, while a fraction remained as oxide; this reprecipitation pathway rationalizes the limited Ag extraction observed in H_2SO_4 when compared with HNO_3.

It should also be noted that Sn was not detected in quantifiable concentrations in the H_2SO_4 leachate under the optimized conditions. SEM-EDS analysis of the leaching residue (Fig. S14, Table S18) confirmed that Sn remained in the solid phase after this step.

The time of extraction is also an important variable to consider. Therefore, a kinetics analysis was performed and is presented in Fig. 5. Although slight increases in metal extraction were observed at longer leaching times, particularly for Cu, most of the extraction of Mn, Cu, Ni, and Zn was achieved within the first 120 min. Therefore, 120 min (2 h) was selected as the operating time as a balance between metal recovery, energy consumption, and process throughput. Ag and Ta extraction remained negligible throughout the studied period.

To better understand the leaching mechanism involved in metal extraction, the widely applied shrinking core kinetic model was employed and adjusted to describe the process. In the shrinking core model, it is assumed that an intermediate layer forms between the unreacted core and the leaching medium. As leaching occurs, the unreacted core recedes toward the center of the particle, resulting in a decrease in the particle's radius. Different linear adjustments can be used, based on the rate-limiting step in the dissolution process: the layer mass transfer control model (Eq. (5)), the surface chemical reaction model (Eq. (6)), and the residual layer diffusion model (Eq. (7)) [52,53].

$$x = k_1 t \quad (5)$$

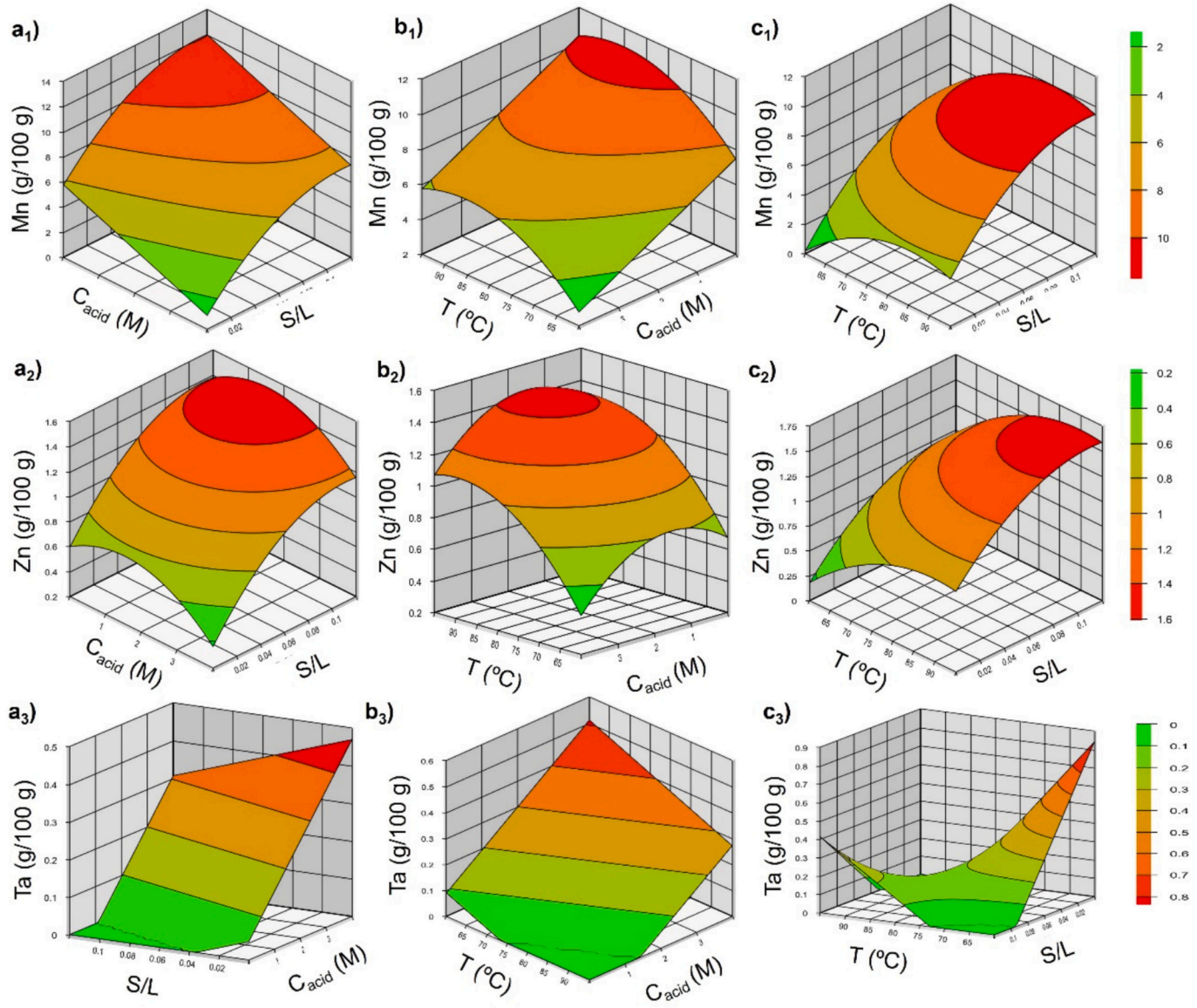

Fig. 4. Response surface plots of H_2SO_4 extraction for Mn (a_1-c_1), Zn (a_2-c_2), and Ta (a_3-c_3), illustrating the combined effects of acid concentration and solid-to-liquid (S/L) ratio (a_1,a_2,a_3), temperature and acid concentration (b_1,b_2,b_3), and temperature and S/L ratio (c_1,c_2,c_3). Mn is presented as a representative example of the extraction behavior also observed for Ni and Cu, whose corresponding plots are provided in Fig. S13 (Supplementary Material).

Table 1
Leaching extraction of metals from TC with H_2SO_4 solution under optimized conditions: [H_2SO_4] = 1.4 M, S/L ratio = 1/10 (w/w), T = 90 °C, t = 2 h.

Element	Mn	Ni	Cu	Zn
Composition (g/100 g of TC)	11.5 ± 0.5	1.75 ± 0.03	7.2 ± 0.3	1.84 ± 0.06

$$1-(1-x)^{\frac{1}{3}}=k_2t \quad (6)$$

$$1-3\cdot(1-x)^{\frac{2}{3}}+2\cdot(1-x)=k_3t \quad (7)$$

where x is the fraction reacted, k_1, k_2, and k_3 are the fitting line slopes, and t is the leaching time (min).

The kinetics data were fitted to the shrinking core linear models assuming no initial extraction (t = 0, x = 0). The parameters were estimated using the leaching obtained up to 120 min, before the leaching efficiency plateau was reached. The constant values and correlation coefficients obtained for each model are shown in Table 2 and Fig. S16.

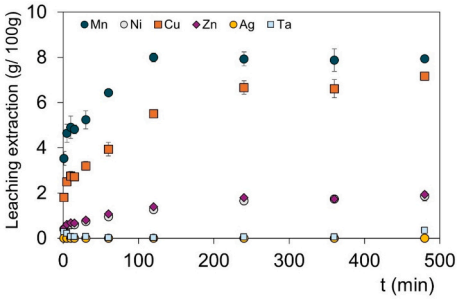

Fig. 5. Effect of time on the leaching extraction of metals from TC using H_2SO_4 at the optimized conditions ([H_2SO_4] = 1.4 M, S/L ratio = 1/10 (w/w) and T = 90 °C).

Although different linearizations of the shrinking core model were

Table 2
Experimental shrinking core model constant values and their respective correlation coefficients for H_2SO_4 leaching of TC ($[H_2SO_4] = 1.4$ M, S/L ratio = 1/10 (*w*/w), $T = 90$ °C, $t = 2$ h).

	Layer mass transfer		Surface chemical reaction		Residual layer diffusion	
Element	k_1 $(min)^{-1}$	R^2	k_2 $(min)^{-1}$	R^2	k_3 $(min)^{-1}$	R^2
Mn	6.36×10^{-3}	0.661	2.67×10^{-3}	0.715	1.52×10^{-3}	0.900
Ni	4.37×10^{-3}	0.764	1.69×10^{-3}	0.800	3.67×10^{-4}	0.922
Cu	3.79×10^{-3}	0.698	1.42×10^{-3}	0.716	4.64×10^{-4}	0.875
Zn	5.11×10^{-3}	0.757	2.04×10^{-3}	0.800	9.40×10^{-4}	0.971

tested, the fits obtained for the residual layer diffusion model were consistently superior, with R^2 values of 0.875–0.971, compared to 0.661–0.757 for layer mass transfer and 0.715–0.800 for surface chemical reaction. This indicates that, while the other models can approximate the data to some extent, residual layer diffusion provides the most accurate description of the leaching kinetics of Mn, Ni, Cu, and Zn. However, the poorer agreement at short times (Fig. S16) suggests a transient stage where the assumptions of the model are not yet valid, since, as Levenspiel (1999) [54] noted, the resistance of the residual layer is absent at the beginning of the reaction but becomes progressively more important as dissolution proceeds. Once the product layer is developed, the residual layer diffusion model accounts well for the experimental data, in line with the response surface results, which also point to diffusion limitations as the dominant factor.

The strong influence of both the solid-to-liquid ratio and temperature observed in the response surfaces is consistent with this kinetic interpretation. In a diffusion-controlled regime, the availability of reactive surface area and the development of a product layer govern the overall rate. At moderate S/L ratios, the higher amount of solid increases contact with the lixiviant, facilitating dissolution. However, the excessive loadings lead to thicker product layers and mass-transfer limitations, which explain the appearance of optimal values rather than continuous improvement. In addition, it cannot be excluded that at very high S/L ratios the decrease in extraction is partly related to acid depletion, since the relative amount of lixiviant per mass of solid becomes insufficient to sustain complete dissolution. A similar trend is observed for temperature: although higher values enhance ion transport and accelerate the initial stages of dissolution, the thickening of the product layer progressively counterbalances this effect, so that the overall rate no longer increases beyond a certain range [54]. This reasoning also explains the role of acid concentration. Increasing the acid concentration does not overcome the diffusional barrier; rather, higher proton availability accelerates the initial dissolution, which promotes a faster build-up and thickening of the product layer. In concentrated sulfuric media, this effect may be reinforced by passivation phenomena, further hindering metal leaching and accounting for the decrease in extraction efficiency observed in the response surfaces [55].

Similar kinetic behaviors were reported in the literature, where the shrinking core model identified residual layer diffusion as the dominant mechanism. Most of these studies concern primary resources, such as the leaching of nickel from low-nickel matte in sulfuric acid [56], the dissolution of copper from molybdenite concentrates in sodium dichromate solution [57], and the leaching of low-grade zinc silicate ore [58]. In addition to primary ores, evidence from recycling processes also points to residual layer diffusion mechanisms. Examples include the oxidative leaching of copper smelting slag in the H_2SO_4-H_2O_2 system [59] and sulfuric acid leaching of Zn from waste metal oxide varistors [60]. These studies confirm that diffusion through the product layer is not only common in mineral systems but also governs the kinetics of several secondary resources, reinforcing the conclusion that the same mechanism controls the leaching of Mn, Ni, Cu, and Zn from TC in this work.

3.1.2. 2^{nd} (HNO_3) leaching step optimization

RSM was also applied to optimize the second leaching step, aiming to selectively extract Ag from the solid residue obtained after H_2SO_4 treatment while minimizing the co-dissolution of Ta. A 2^2 CCRD was used to evaluate the effects and interaction of two independent variables, i.e., HNO_3 concentration (0.6–3.4 M) and temperature (49–95 °C). The solid-to-liquid ratio (1/10 *w*/w) and contact time (2 h) were maintained constant. The complete experimental matrix and responses are provided in the Supplementary Material (Tables S19–S23, Figs. S17-S20). Model fitting was evaluated using analysis of variance (ANOVA), with both models demonstrating satisfactory predictive accuracy at the 95% confidence level, as indicated by coefficients of determination of $R^2 = 0.96$ for Ta and $R^2 = 0.87$ for Ag, and by F-calculated > F-tabulated. These results confirm the reliability of the models in describing the experimental data.

The influence of the operational variables on Ag and Ta extraction is illustrated in the response surface plots Fig. 6 and corroborated by the Pareto charts (Figs. S17 and S19). For Ag, both HNO_3 concentration and temperature had a positive effect on extraction, with both variables showing a similar level of significance. However, the quadratic terms for both factors were also significant and negative, indicating the existence of an optimal region beyond which extraction yields declined, consistent with the presence of a maximum in the response surface. The interaction term also exhibited a negative effect, indicating that the simultaneous increase in both variables resulted in a reduction in extraction efficiency. Overall, Ag extraction was favored under intermediate-to-high acid concentrations and temperatures, particularly in the range of 2.0–2.5 M HNO_3 and 70–90 °C.

These contrasting behaviors enabled the identification of a selective leaching window, in line with the objective of maximizing Ag extraction while minimizing Ta dissolution. Moderate leaching conditions proved sufficient to enhance Ag recovery while maintaining minimal Ta solubilization. Based on these trends, the optimal conditions for the selective leaching of Ag from the solid residue were determined to be 72 °C and 2.0 M HNO_3. Under these conditions, the experimental extraction of (1.1 ± 0.2) g/100 g for Ag and (0.159 ± 0.009) g/100 g for Ta was in good agreement with the predicted trends, supporting the suitability of the selected leaching parameters.

The extraction behavior of Ag is consistent with what is expected in nitrate media. Nitric acid is a strong oxidizing lixiviant that converts metallic oxide or sulfide Ag into soluble Ag^+ (as $AgNO_3$), so increasing HNO_3 concentration initially promotes dissolution. At higher concentrations, however, the efficiency of Ag extraction decreases, as also observed in previous kinetic studies of silver dissolution in nitric acid [61,62]. This decline was attributed to the formation of a saturated $AgNO_3$ film at the solid–liquid interface and the reduced availability of catalytic HNO_2 formed in the reaction. These phenomena account for the negative quadratic effect of acid concentration and explain the presence of an optimum region in the response surfaces. Previous studies on silver dissolution in nitric acid generally reported exclusively positive effects of temperature on extraction; however, these investigations were restricted to lower temperature ranges (25–65 °C) [61–63], which makes the comparison with the present results less direct. Different kinetic regimes were also identified depending on the experimental conditions: at high acid concentrations, the process was associated with mass-transfer limitations [62], whereas in others, surface chemical reaction was identified as the controlling step [61]. Additionally, silver recovery from spent silver oxide button cells was described as an intermediate-controlled mechanism, with both nitric acid concentration and temperature exerting a positive effect on the dissolution process [63]. Taken together, these studies demonstrate that the rate-controlling step in silver dissolution is not universal but highly dependent on the

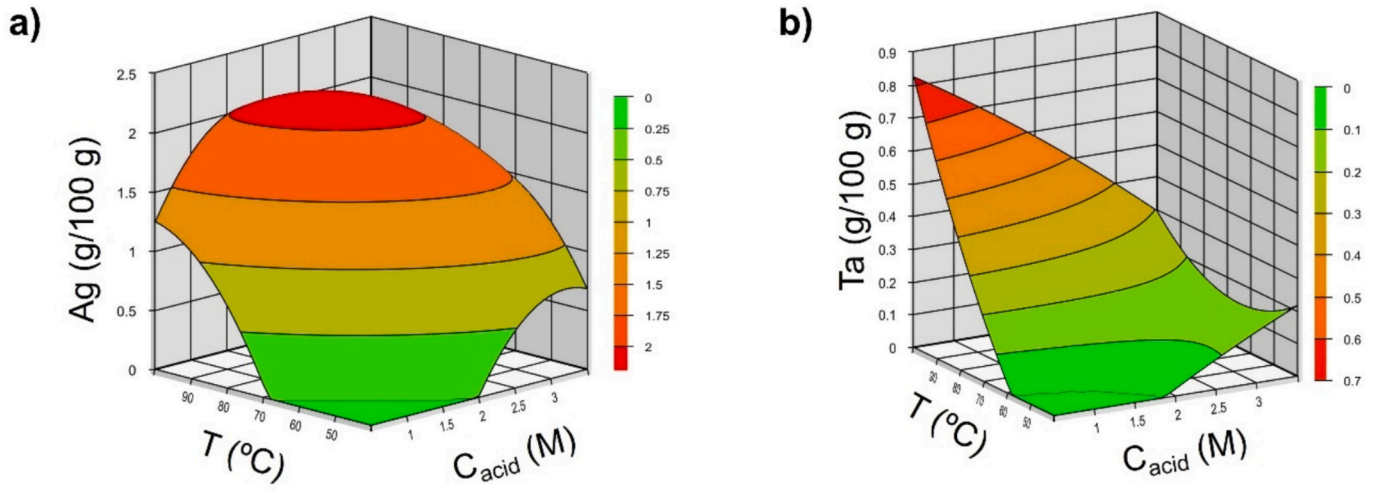

Fig. 6. Response surface plots of HNO_3 extraction of Ag (a) and Ta (b) with the combined effects of concentration of acid and temperature.

leaching window and the material investigated.

In contrast, Ta remains largely solid in nitrate media, since HNO_3 provides no strong complexation pathway for Ta in the absence of fluoride; as a result, increasing HNO_3 concentration or temperature within the studied range does not meaningfully promote Ta dissolution. These contrasting behaviors define a selective window — intermediate-to-high acid concentration (≈2.0–2.5 M) and elevated temperature (≈70–90 °C) — that maximizes Ag recovery while keeping Ta in the solid, matching the experimentally validated optimum.

The residual solid after HNO_3 leaching was analyzed by SEM-EDS (Fig. S21, Table S24) and XRD (Fig. S22). SEM-EDS analysis confirms that Ag was effectively removed by HNO_3 leaching, while Ta remained as the main component. The final solid residue contains (79 ± 2) wt% of Ta, which increases to (85 ± 3) wt% when Zr is excluded, since this element can be removed from the process by optimizing the milling step. The reported purity values were estimated from multiple SEM-EDS measurements performed at different regions of the sample to minimize local heterogeneity effects.

Considering the estimated Ta content of the initial material obtained by SEM-EDS analysis (~42 wt%), the combined Ta loss during the H_2SO_4 and HNO_3 leaching steps was approximately 0.191 g/100 g TC, corresponding to less than 0.5 wt% of the initial Ta content. These results confirms that Ta was effectively retained in the solid phase throughout the process. Likewise, Sn was not leached in quantifiable amounts during the HNO_3 leaching step. SEM-EDS analysis of the final residue (Fig. S21, Table S24) confirmed its presence, indicating that Sn remained associated with the Ta-rich solid throughout the process. If higher Ta purities are required, additional purification steps targeting Sn-containing phases could be implemented after the leaching process. For example, sequential HCl and NaOH treatments have been reported as an effective approach for Sn removal during the upgrading of Ta- and Nb-rich materials from tin slag [64]. However, the development and optimization of an additional Sn-removal step was beyond the scope of the present work, which focused on the selective recovery of metals and the production of a Ta-rich solid.

The XRD pattern supports these results, showing Ta as the dominant crystalline phase and the continued presence of Sn and ZrO_2 (contaminant from the milling process). It is important to highlight that Zr was not detected in the leachate during any of the leaching steps. This is consistent with its known resistance to leaching, as Zr requires either a large excess of concentrated sulfuric acid or the presence of toxic fluoride ions to be effectively solubilized [51]. Therefore, while Zr acts as a contaminant introduced during sample preparation, it remains inert under the conditions applied in this process. The absence of detection of Ag-containing phases further confirms the success of the second leaching step of the TC.

Although the recovered tantalum-containing solid does not correspond to high-purity tantalum, it can be directly used as a feedstock for downstream tantalum processing routes. In contrast to primary tantalum concentrates, which typically contain around 30 wt% Ta_2O_5 [65] and require extensive chemical upgrading, the proposed process delivers a highly enriched oxide-based material, substantially reducing the need for further beneficiation.

3.2. Selective recovery of leached metals

3.2.1. Mn, Zn, Cu and Ni recovery from H_2SO_4 solution

The final H_2SO_4-leachate (composition in Table S25) was subjected to a sequence of separation steps to recover the metals individually as shown in Fig. 7.

Initially, $KMnO_4$ was added to promote the precipitation of Mn. This treatment oxidized Mn to insoluble MnO_2 and can be generally represented by Eq. (8):

$$3Mn^{2+} + 2MnO_4^- + 2H_2O \rightleftharpoons 5MnO_2 + 4H^+ \quad (8)$$

$KMnO_4$ was selected because it provides direct, rapid, and efficient separation under acidic conditions, eliminating the need for pH adjustment (original pH of 0.15) [66]. Mn was almost completely recovered (97.29 ± 0.03) % while the other metals remained in the liquid phase (Fig. S23). Based on the variation of metal concentrations in the liquid phase before and after precipitation, Mn corresponded to approximately 98 wt% of the metals recovered in the brown solid obtained.

Next, 0.4 M of CYANEX® 272 dissolved in *n*-dodecane was used to

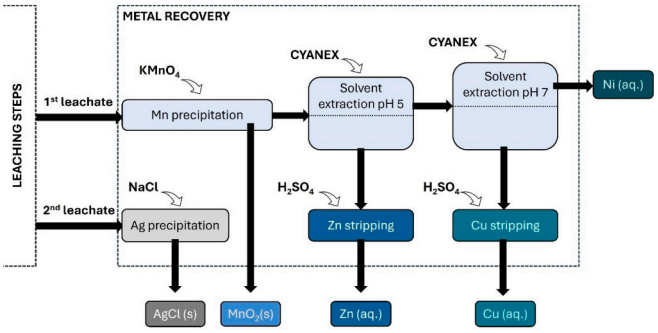

Fig. 7. Schematic representation of the metal recovery steps following the two-step leaching process (Fig. 3) for metals recovery from TC.

extract the remaining metals from the aqueous phase. CYANEX® 272 is an acidic organophosphorus extractant whose active component is a dialkyl phosphinic acid, and metal ions are recovered through a cation-exchange mechanism. CYANEX® 272 is reported to be fully miscible with both aliphatic and aromatic diluents and to display excellent thermal and hydrolytic stability. CYANEX® 272 was selected as an extractant due to its well-established efficiency in separating base metals from sulfate media through a pH-dependent cation-exchange mechanism. Building on this known behavior, the present work applies CYANEX® 272 and explores its selective extraction performance for Zn, Cu, and Ni under controlled and optimized conditions [33]. The extraction of divalent cations with CYANEX® 272 follows a cation-exchange mechanism that can be expressed as in Eq. (9):

$$M^{2+}_{(aq)} + 2(RH)_{(org)} \rightleftharpoons M(R_2)_{(org)} + 2H^{+}_{(aq)} \quad (9)$$

where M^{2+} represents the metal ion in the aqueous phase, RH is the phosphinic acid extractant, and the subscripts "*aq*" and "*org*" refer to the aqueous and organic phases, respectively. In this equilibrium, metal ions are transferred into the organic phase by displacing protons originally bound to the extractant [67]. Consequently, the distribution of metals is strongly governed by the proton concentration of the solution: at low pH values, the high concentration of H^+ suppresses metal uptake, while increasing the pH reduces proton competition and promotes the formation of stable metal–extractant complexes in the organic phase [33].

Different pH values were evaluated to determine the best conditions for extracting each metal, from 0.15 (original) to 8.5. The pH was adjusted using a 14 M NH_3 solution, which was selected because ammonia both prevents precipitation by increasing the solubility of the corresponding metal sulphates at higher pH and promotes selective separation through the formation of aqueous metal-ammonia complexes that influence the distribution of each cation between phases [68]. The pH dependency behavior is illustrated in Fig. 8a. At low pH values (≤ 3), there is negligible transfer to the organic phase. With increasing pH, competition from protons decreases, and Zn is the first to be efficiently extracted, reaching almost complete transfer at pH 5. This agrees with its higher affinity for the phosphinic acid extractant compared with Cu and Ni [33,69]. At intermediate pH values (≈ 6), Cu extraction increases sharply, while Ni remains largely in the aqueous phase. Only at higher pH values (≥ 8) does Ni show substantial extraction, consistent with literature reports [33,70]. This sequential shift demonstrates the feasibility of stepwise separation, where Zn can be selectively recovered at lower pH, Cu at intermediate pH, and Ni at higher pH. Therefore, two solvent extraction steps were performed in the process (Fig. 7), and the results are shown in Fig. 8b-c.

The first solvent extraction step, aimed at extracting Zn, was performed at pH 5. The result is shown in Fig. 8b, and (94.33 ± 0.06) % of Zn was extracted to the organic phase, while the other metals remained in the aqueous phase. Following this, Zn was stripped into a solution of H_2SO_4, and the different concentrations were analyzed (Fig. 8c). A concentration of 0.1 M H_2SO_4 was able to strip 100% of the Zn with a purity of 93 wt%. Sulfuric acid was selected as the stripping agent because it is the most widely applied acid in hydrometallurgy and the acid of choice in electrolytes for the electrowinning and electrorefining of several base metals, thereby facilitating integration with downstream recovery steps [71].

Another extraction with the mixture of 0.4 M CYANEX® 272 in dodecane was done at pH 7. The result is shown in Fig. 8b. 100% of Cu was extracted to the organic phase while Ni remained in the aqueous phase with a purity of 99 wt%. In the sequence, Cu was stripped to a solution of H_2SO_4. Different concentrations were analyzed (Fig. 8c), and a purity of 94 wt% Cu in the aqueous phase was achieved with 0.5 M H_2SO_4.

While previous studies [69] reported the recovery of Zn and Cu from CYANEX® 272 using sulfuric acid, these processes typically require multiple stripping stages and/or higher acid concentrations under different operating conditions, including lower extractant concentrations and continuous multistage configurations. In contrast, the present work demonstrated efficient stripping behavior, achieving complete Zn recovery and high Cu recovery in a single stripping stage using comparatively diluted H_2SO_4 solutions under the investigated batch conditions.

3.2.2. *Ag recovery from HNO_3 solution*

Following the HNO_3 leaching step, NaCl was added to the leachate

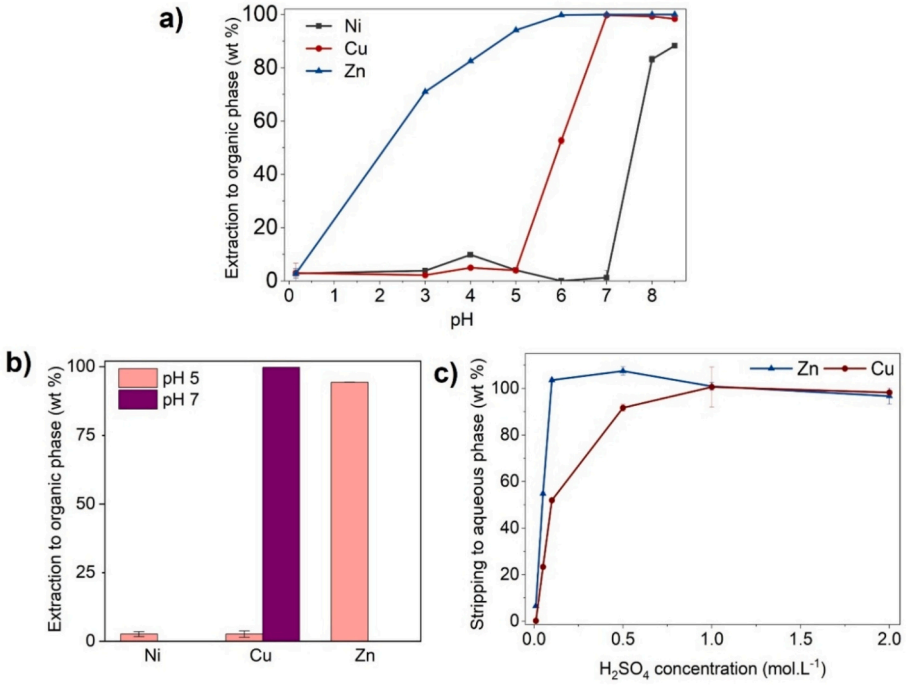

Fig. 8. Extraction of metals using 0.4 M CYANEX® 272 and dodecane as a function of pH (a), and at pH 5 and 7 (b). Stripping of metal as a function of H_2SO_4 concentration in aqueous solution of Zn and Cu (c). Ratio between organic and aqueous solution is 1/1 *w*/w in all cases.

(molar ratio of 1.1 NaCl: 1 Ag) to induce the precipitation of AgCl, as can be seen in Fig. 7. Upon NaCl addition, Ag precipitation occurs according to Eq. (10):

$$Ag^{+} + Cl^{-} \rightleftharpoons AgCl \quad (10)$$

Sodium chloride was selected as a precipitating agent because it provides a readily available and inexpensive source of chloride ions, and AgCl is extremely insoluble in aqueous media (0.00019 g/100 g at 25 °C) [72]. The formation of AgCl was confirmed by XRD analysis (Fig. S24), which showed only the characteristic diffraction peaks of AgCl and no detectable secondary crystalline phases. The precipitate exhibited an Ag recovery of (96.2 ± 0.4) wt% with a purity of (98 ± 6) wt%, demonstrating the high selectivity of the precipitation step (Table S26). The small fraction of unrecovered Ag is likely associated with residual dissolved Ag species remaining in solution after precipitation. The remaining impurities were mainly Ni and Mn, which are expected to remain soluble as chloride species under the investigated conditions. Therefore, their presence is likely related to entrainment of the mother liquor and could be further reduced through additional washing steps if higher AgCl purities are required.

4. Conceptual process and economic/life cycle assessments

The results obtained led to the conceptual development of a process that enables the extraction and recovery of metals from TC, illustrated in Fig. 9.

The process consists of three main stages: (1) pretreatment, (2) extraction, and (3) purification. In the extraction stage, two steps are present: H_2SO_4 and HNO_3 leaching. The purification step includes Mn and Ag precipitation, as well as Zn and Cu solvent extraction leaving Ni in the aqueous phase. In Fig. 9, the black continuous arrows represent the steps developed in this work, while the black dashed lines (i.e. the organic phase recycling) represent conceptual steps that were considered for the LCA but not tested. Moreover, in each stage, the inlets and outlets are described in terms of their composition, purity, and global metal recovery. The overall recoveries achieved were 97% for Mn, 84% for Ni, 91% for Cu, 91% for Zn, 96% for Ag, and 99.6% for Ta. A detailed material balance for all process streams, normalized to the treatment of 1 kg of TC, is provided in the Supplementary Information (Table S27).

Regarding industrial implementation, additional process engineering considerations, including reagent handling and pH-control strategies, should be evaluated in future scale-up studies. In particular, the use of 14 M NH_3 in the present work was selected to minimize dilution during laboratory-scale pH adjustment and is not an intrinsic requirement of the process. Under the investigated conditions, the required NH_3 solution corresponds to less than 5% of the leachate mass. Therefore, more dilute ammonia solutions could be employed at industrial scale with only a limited increase in process volume, while potentially improving operational safety. Ammonia-containing process streams should also be considered during future process engineering studies, including the implementation of wastewater treatment integration and ammonium sulphate recovery strategies according to the final process configuration. The presence of ammonia-containing streams was already considered in the LCA inventory and therefore contributes to the environmental impact assessment of the proposed process.

Furthermore, although new capacitors were used in this study, end-of-life capacitors from real waste streams may exhibit different degrees of oxidation, contamination, or degradation, which could influence process performance and warrant further investigation.

To evaluate the environmental benefits of the proposed recovery process, a LCA was performed. The results obtained for the processing of 1 kg of TC were compared with those of producing the same quantities of metals from primary sources (Table S28). Inventory data for primary metal production was sourced from the ecoinvent database version 3.11 [42].

The LCA results show that the proposed recovery process offers significant environmental advantages compared to primary metal production. Across all impact categories evaluated, the recovery process leads to substantial reductions. Climate change and acidification are reduced by approximately 86% and photochemical ozone formation by 94%. Eutrophication impacts are also notably lower, with reductions of around 97% for marine ecosystems and 96% for freshwater. In terms of resource consumption, the recovery process reduces fossil resource use by approximately 78%, while the impact on mineral and metal resource use is reduced by more than 99.9%. These results underscore the significant environmental benefits of the recovery approach, rendering it a more sustainable alternative to conventional primary metal production and supporting the development of circular economy strategies in the electronics sector.

When analyzing the environmental impacts associated with each step of TC recycling, the purification stage clearly stands out as the primary contributor (Fig. 10a). Zn and Ni/Cu solvent extraction steps account for a substantial share of the total impact, contributing approximately 20–47%, and 39–49%, respectively. The solvent extraction step for Ni and Cu recovery emerges as the major hotspot in all environmental impact categories, largely driven by the production of CYANEX® 272, as well as H_2SO_4 production in the case of the acidification category. The production of CYANEX® 272 is also the main cause of impacts in the Zn solvent extraction.

Fig. 10b highlights the contributions of individual metal productions in the primary production route. Ta is the dominant contributor across most impact categories. However, in mineral and metal resources use, AgCl production takes the lead, indicating a relatively higher environmental burden in this category. Since Ta dominates the environmental footprint of the primary route, its recovery from waste effectively offsets these impacts, turning a critical waste stream into a sustainable secondary source. This not only eliminates the need for high-impact primary extraction but also closes the loop for one of the most critical elements in modern electronics, reinforcing the circularity and overall sustainability of the proposed process.

To assess the economic feasibility, a preliminary cost–benefit analysis was performed, focusing specifically on the reagent costs incurred in processing 1 kg of TC as shown in Fig. 9. The costs and returns considered are shown in Table S29 and Table S30, respectively. Considering average values for the last years, the process costs €6.99 and returns €84.36, yielding a gross margin of €77.37 per kg of TC. When individual process outputs are considered, the solid Ta oxide stream obtained is economically decisive since it accounts for approximately 99% of the total revenue. A stepwise breakdown (Table S31) indicates that most auxiliary recovery steps, namely MnO_2 precipitation and solvent extraction stages, introduce additional operating costs that are higher than their respective returns. In contrast, Ag recovery via AgCl precipitation is economically self-sustaining, as the associated operating cost is fully compensated by the value of the recovered product.

Given that tantalum oxide accounts for approximately 99% of the total process revenue, the economic robustness was assessed as a function of Ta_2O_5 market variability. Using the minimum and maximum Ta_2O_5 prices reported over the past five years (Table S30), the process remains profitable across the entire price range, with estimated gross margins between €71.29 and €89.92 per kg of TC. This sensitivity analysis demonstrates that the economic performance of the proposed process is largely insensitive to short-term market fluctuations, supporting its robustness and potential applicability under realistic operating conditions.

Building on the techno-economic assessment, which identified Ta_2O_5 and AgCl recovery as the only economically viable stages of the process, a scenario-based LCA was carried out to investigate the environmental implications of restricting the flowsheet to these steps. This approach enables a direct evaluation of how process simplification, guided by economic feasibility, affects the overall environmental performance, while maintaining a consistent system boundary definition across

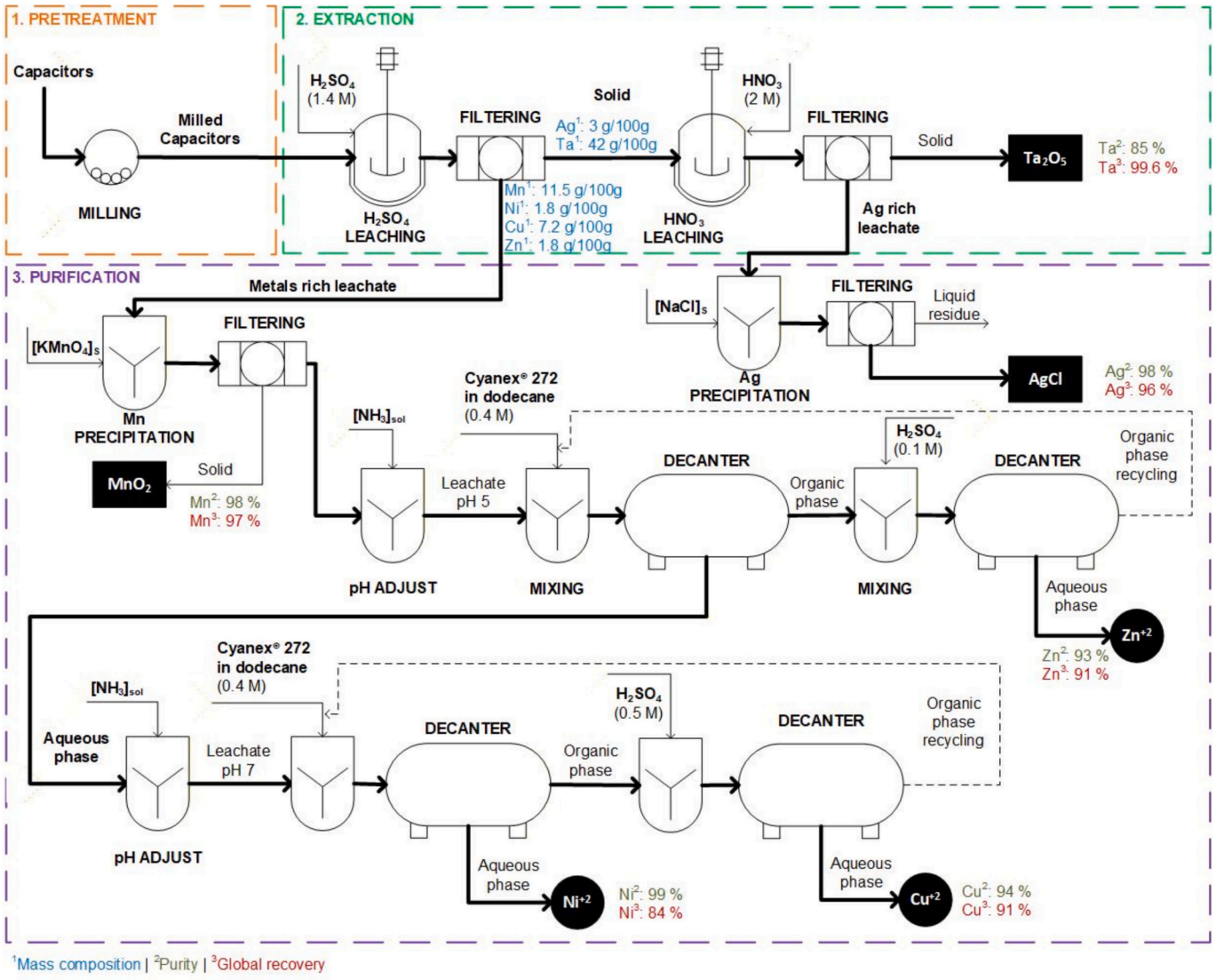

Fig. 9. Process diagram for the recycling of TC.

scenarios.

Three LCA scenarios were therefore evaluated, including the full process with all separation and purification stages (1), a reduced configuration limited to Ta_2O_5 recovery up to the HNO_3 leaching step (2), and a streamlined route combining Ta_2O_5 recovery with AgCl precipitation (3). The results comparing the relative environmental impacts of the proposed scenarios compared with the conventional primary metal production (100%) are shown in Fig. 11.

The results reveal that the scenario considering only tantalum recovery exhibits slightly higher relative environmental impacts compared with primary metal production across most impact categories when compared to the scenario that includes silver recovery. Although this outcome may appear counterintuitive at first glance, it can be rationalised by examining the distribution of environmental burdens across recovered products (Fig. 10b). When silver is not recovered, the impacts associated with reagent consumption, energy use, and upstream processing remain entirely attributed to tantalum, resulting in higher impacts per functional unit. In contrast, including silver recovery allows these burdens to be shared between two valuable products, thereby improving overall resource efficiency. Moreover, the AgCl precipitation step introduces only a limited marginal environmental burden, mainly associated with NaCl consumption and minor additional processing requirements. This additional impact is largely outweighed by the environmental benefit of recovering silver, a high-value metal whose extraction from primary resources is associated with significant environmental pressures.

This observation does not undermine the environmental relevance of the full process; rather, it highlights the role of scenario-based allocation in shaping impact interpretation and demonstrates how selective recovery strategies can enhance overall process efficiency. The complete flowsheet remains a necessary reference case, as it captures the cumulative environmental burdens associated with all recovery and purification stages and provides a comprehensive baseline for comparison. In this context, the reduced and streamlined scenarios should be regarded not as alternative process proposals, but as analytical tools that help identify where environmental and economic performance can be most effectively improved through process intensification and targeted optimisation. Further improvements could be achieved by reusing and recirculating the aqueous phases containing Zn, Cu, and Ni, allowing these metals to be progressively concentrated into more defined outlet streams without modifying the overall process configuration. Such an approach would increase the effective metal concentration in the final aqueous products while reducing dilution, reagent consumption, and downstream treatment requirements. This perspective reinforces that the complete flowsheet remains a viable and promising framework, with clear opportunities for optimisation through internal stream

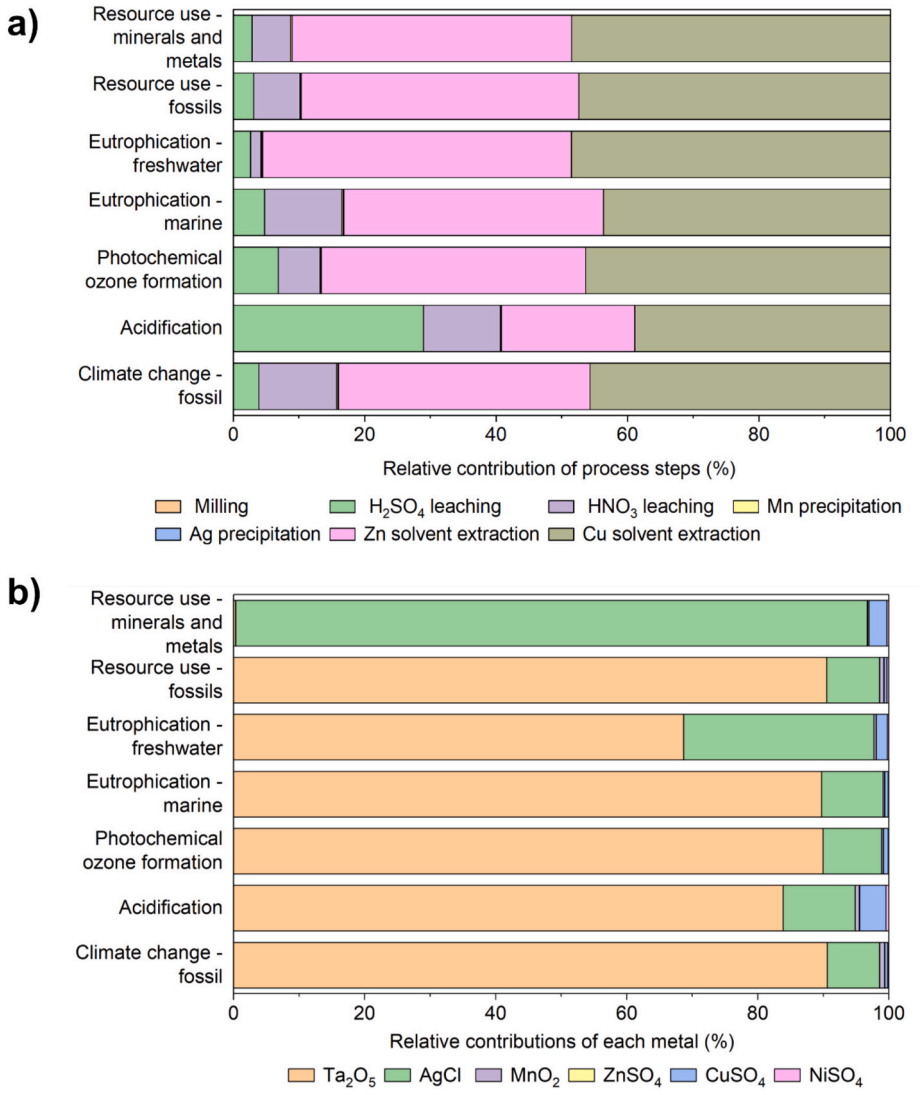

Fig. 10. Relative contributions to the LCA results for (a) each step of the metal recovery process from TC, and (b) each metal in the primary production route, across seven environmental impact categories.

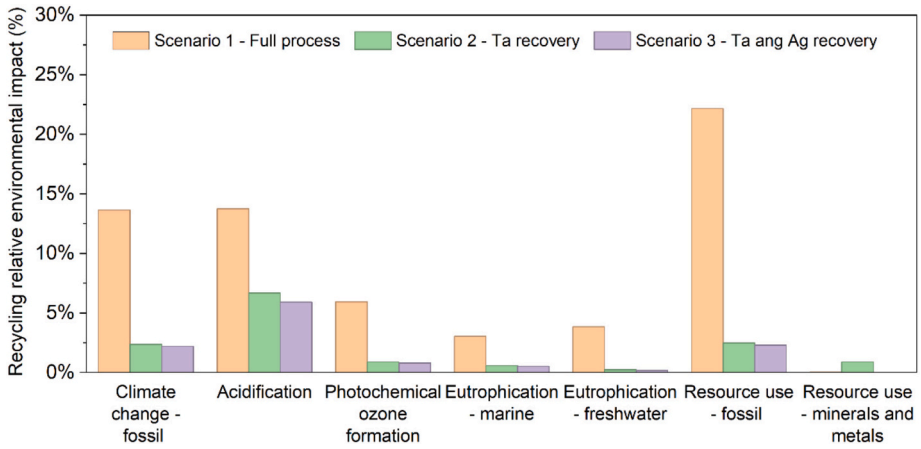

Fig. 11. Relative environmental impacts of the three different scenarios compared with the conventional primary metal production (100%).

management rather than fundamental process redesign.

Beyond economic considerations, the proposed process presents several operational advantages, including direct recovery of Ta_2O_5 as a solid at the leaching stage, a fluoride-free flowsheet based on readily available reagents, and the use of a recyclable organic phase in solvent extraction. In addition, aqueous side streams containing Ag, Mn, Zn, and

Cu can be reused and progressively concentrated according to market requirements, offering flexibility for process operation and scale-up. Compared to primary tantalum mining, which typically yields concentrates containing less than 30 wt% Ta_2O_5 [65], the process produces a highly enriched tantalum-containing solid (~85 wt% Ta), reducing downstream purification needs. Consistent with these features, the LCA confirms significant environmental benefits relative to primary production. Overall, while some by-product recovery steps are not economically attractive when considered individually, the process remains economically viable as a whole and environmentally favourable within a circular-economy framework.

The favourable technical, economic, and environmental outcomes obtained in this study suggest that the proposed approach may have relevance beyond the specific capacitor type investigated. While this study focused on a commercial 470 μF, 6.3 V D-case tantalum capacitor, the recovery strategy is based on the chemical behavior of the constituent metals and is expected to be applicable to tantalum capacitors with similar compositions. Future work should evaluate the performance of the process using capacitors from different manufacturers and with different specifications.

5. Conclusion

This study presents a hydrometallurgical process for the selective recovery of Ta, Ag, and remaining transition metals from TC. By avoiding the dissolution of Ta, the proposed method enables the efficient separation and purification of this metal, as well as Ag, Mn, Ni, Cu, and Zn, through a combination of acid leaching, precipitation, and solvent extraction steps. Optimization through response surface methodology ensured high recovery efficiencies, with purities above 93% for all recovered metals.

The sequential leaching approach, employing sulfuric acid for base metal extraction and nitric acid for selective silver recovery, proved effective in maximizing metal yields while maintaining Ta oxide in the solid residue. Mn was nearly completely precipitated using $KMnO_4$, while Zn and Cu were successfully separated by pH-controlled solvent extraction using CYANEX® 272 in dodecane. Silver was recovered as AgCl.

The process was consolidated into a conceptual flowsheet and evaluated through LCA. LCA results demonstrated that the proposed recycling route offers substantial environmental advantages over primary metal production, reducing impacts by up to 99.9% across key categories. The purification stage was identified as the primary contributor to residual impacts, primarily due to the production of chemical reagents. Nonetheless, the overall process supports circular economy strategies by enabling the recovery of critical and valuable metals from e-waste, thereby reducing the environmental burden. A preliminary cost analysis confirms the economic feasibility of the proposed process.

These results validate the technical feasibility and sustainability of the proposed process, offering a viable solution for addressing the growing e-waste challenge while safeguarding critical material supply chains.

CRediT authorship contribution statement

Flavia N. Braga: Writing – original draft, Validation, Investigation, Formal analysis, Data curation. **Maria C. Hespanhol:** Writing – review & editing, Validation, Supervision, Methodology, Investigation, Formal analysis, Data curation, Conceptualization. **Ana M. Ferreira:** Writing – review & editing, Formal analysis. **Ana C.R.V. Dias:** Writing – review & editing, Writing – original draft, Formal analysis. **Helena Passos:** Writing – original draft, Validation, Supervision, Resources, Funding acquisition. **Nicolas Schaeffer:** Writing – review & editing, Supervision, Resources, Conceptualization. **João A.P. Coutinho:** Writing – review & editing, Supervision, Resources.

Declaration of competing interest

The authors declare that they have no known competing financial interests or personal relationships that could have appeared to influence the work reported in this paper.

Acknowledgments

This work was financially supported by national funds through FCT – Fundação para a Ciência e a Tecnologia, I.P., within the scope of the project PlatILPlus (2022.04478.PTDC, DOI: 10.54499/2022.04478.PTDC). This work was further financially supported by Fundação para a Ciência e a Tecnologia, I.P. /MCTES through national funds: LSRE-LCM, UID/50020/2025 (DOI: 10.54499/UID/50020/2025); ALiCE, LA/P/0045/2020 (DOI: 10.54499/LA/P/0045/2020); and CICECO-Aveiro Institute of Materials, UID/50011/2025 & LA/P/0006/2020 (DOI 10.54499/LA/P/0006/2020). N.S. acknowledges the European Research Council (ERC) for the starting grant ERC–2023–StG–101116461. A.M.F. and F.B. acknowledge FCT for the researcher contract CEECIND/00361/2022 (DOI: 10.54499/2022.00361.CEECIND/CP1720/CT0020) and the Ph.D. grant 2023.01749.BD (DOI:10.54499/2023.01749.BD), respectively. A.C.D. also acknowledges funding by national funds through FCT – Fundação para a Ciência e a Tecnologia I.P., under the project CESAM – Centro de Estudos do Ambiente e do Mar, references UID/50017/2025 (doi.org/10.54499/UID/50017/2025) and LA/P/0094/2020 (doi.org/10.54499/LA/P/0094/2020). M.C.H. thanks Conselho Nacional de Desenvolvimento Científico e Tecnológico (CNPq: 305649/2021-3; 407799/2022-2) and Fundação de Amparo à Pesquisa do Estado de Minas Gerais (FAPEMIG: RED-00161-23, APQ-01134-23).

Appendix A. Supplementary data

Supplementary data to this article can be found online at https://doi.org/10.1016/j.susmat.2026.e02136.

Data availability

Data will be made available on request.

References

[1] C.P. Baldé, R. Kuehr, T. Yamamoto, R. McDonald, E. D'Angelo, S. Althaf, G. Bel, O. Deubzer, E. Fernandez-Cubillo, V. Forti, V. Gray, S. Herat, S. Honda, G. Iattoni, D.S. Khetriwal, V. Luda di Cortemiglia, Y. Lobuntsova, I. Nnorom, N. Pralat, M. Wagner, The Global e-waste Monitor 2024. https://www.itu.int/itu-d/sites/environment, 2024.

[2] L.M. Martelo, P.M.S. Sousa, M.A.D. Silva, H.M.V.M. Soares, A critical updated review of all stages of the tantalum recycling chain from waste of tantalum capacitors, Chem. Eng. J. 472 (2023) 144917, https://doi.org/10.1016/j.cej.2023.144917.

[3] Precedence Semiconductor and Electronic Experts, Capacitor Market Size and Forecast 2024 to 2034. https://www.precedenceresearch.com/capacitor-market, 2024 (accessed January 3, 2025).

[4] L. Smith, T. Ibn-Mohammed, S.C.L. Koh, I.M. Reaney, Life cycle assessment and environmental profile evaluations of high volumetric efficiency capacitors, Appl. Energy 220 (2018) 496–513, https://doi.org/10.1016/J.APENERGY.2018.03.067.

[5] M. Agrawal, R. Jha, R. Singh, K.K. Singh, Flow and stock estimation of tantalum for sustainable supply chain, Sustainable Prod. Consumption 34 (2022) 385–394, https://doi.org/10.1016/J.SPC.2022.10.002.

[6] M. Agrawal, R. Singh, M. Ranitović, Z. Kamberovic, C. Ekberg, K.K. Singh, Global market trends of tantalum and recycling methods from waste tantalum capacitors: a review, Sustain. Mater. Technol. 29 (2021) e00323, https://doi.org/10.1016/J.SUSMAT.2021.E00323.

[7] R. Sharma, H. Kumar, G. Kumar, S. Sharma, R. Aneja, A.K. Sharma, R. Kumar, P. Kumar, Progress and challenges in electrochemical energy storage devices: fabrication, electrode material, and economic aspects, Chem. Eng. J. 468 (2023) 143706, https://doi.org/10.1016/J.CEJ.2023.143706.

[8] L. Xia, X. Wei, H. Wang, F. Ye, Z. Liu, Valuable metal recovery from waste tantalum capacitors via cryogenic crushing-alkaline calcination-leaching process, J. Mater. Res. Technol. 16 (2022) 1637–1646, https://doi.org/10.1016/j.jmrt.2021.12.104.

[9] Z. Chen, B. Niu, L. Zhang, Z. Xu, Vacuum pyrolysis characteristics and parameter optimization of recycling organic materials from waste tantalum capacitors,

J. Hazard. Mater. 342 (2018) 192–200, https://doi.org/10.1016/J.JHAZMAT.2017.08.021.
[10] N.T. Nassar, Shifts and trends in the global anthropogenic stocks and flows of tantalum, Resour. Conserv. Recycl. 125 (2017) 233–250, https://doi.org/10.1016/J.RESCONREC.2017.06.002.
[11] J. Ma, X. Guo, H. Xue, K. Pan, C. Liu, H. Pang, Niobium/tantalum-based materials: synthesis and applications in electrochemical energy storage, Chem. Eng. J. 380 (2020) 122428, https://doi.org/10.1016/J.CEJ.2019.122428.
[12] European Commission, Study on the critical raw materials for the EU 2023 – Final report, 2023, https://doi.org/10.2873/725585.
[13] B. Choi, B. Domínguez, A. D'Souza, H. Khadse, A. Kunkel, S. Nagarajan, T. Necke, R. Peche, M. Revello, J. Rossa, F. Sauer, S. Huyer, O. Schulz, S. Vorwerg, C. Walls, M. Wickleder, G. Beck, Sustainable recycling process for tantalum recovery from printed circuit boards, Resour. Conserv. Recycl. 198 (2023) 107201, https://doi.org/10.1016/J.RESCONREC.2023.107201.
[14] W. Qin, Z. Nian, T. Cuili, C. Yanhong, Method for recovering tantalum, silver and manganese in waste and old tantalum capacitor, CN Pat.,103194604A, 2012.
[15] X. Zheniming, B. Niu, Z. Chen, Method for preparing oxygen tantalum nitride photocatalytic material by means of waste tantalum capacitors, , CN Pat.,. 106276827A, 2017.
[16] B. Niu, Z. Chen, Z. Xu, An integrated and environmental-friendly technology for recovering valuable materials from waste tantalum capacitors, J. Clean. Prod. 166 (2017) 512–518, https://doi.org/10.1016/J.JCLEPRO.2017.08.043.
[17] K. Mineta, T.H. Okabe, Development of a recycling process for tantalum from capacitor scraps, J. Phys. Chem. Solid 66 (2005) 318–321, https://doi.org/10.1016/J.JPCS.2004.06.060.
[18] Z. Xu, Z. Liu, B. Niu, Method for recovering tantalum, silver, nickel and iron from waste tantalum capacitor, CN Pat., 106048231A, 2016.
[19] K. Vutova, V. Vassileva, E. Koleva, E. Georgieva, G. Mladenov, D. Mollov, M. Kardjiev, Investigation of electron beam melting and refining of titanium and tantalum scrap, J. Mater. Process. Technol. 210 (2010) 1089–1094, https://doi.org/10.1016/J.JMATPROTEC.2010.02.020.
[20] M. Yoshida, K. Matsuzaki, T. Aoki, R. Ishii, Method for Recovering Tantalum., US Pat., 2013014611A1, 2013.
[21] G.G. Lee, Method for Recycling Tantalum., KR Pat., 20170058211A, 2017.
[22] E. Wansi, P. D'Ans, L. Gonda, T. Segato, M. Degrez, Waste Management of Discarded Cell Phones and Proposal of material recovery techniques, Procedia CIRP 69 (2018) 974–979, https://doi.org/10.1016/J.PROCIR.2017.11.011.
[23] W.-S. Chen, H.-J. Ho, K.-Y. Lin, Hydrometallurgical process for tantalum recovery from epoxy-coated solid electrolyte tantalum capacitors, Materials 12 (2019) 1220, https://doi.org/10.3390/ma12081220.
[24] F. Bastin, A. Janssen, Y. Lolivier, M. Masalskas, A. van Rechem, P. D'Ans, Exploration of alternative routes for recycling critical metals from waste PCB and tantalum capacitors, Procedia CIRP 90 (2020) 437–442, https://doi.org/10.1016/J.PROCIR.2020.01.112.
[25] J.J. Gi, K.W. Baek, L.J. Cheon, C.Y. Seo, Method for Recovering Tantalum Anode from Waste Tantalum Capacitor, KR Pat., 20040072779A, 2004.
[26] T. Yumoto, Method for Recovering Tantalum from Electronic Substrates, , JP Pat., 2009221514A,, 2009.
[27] M. Agrawal, R. Singh, K.K. Singh, Recovery of silica-free tantalum from epoxy-coated tantalum capacitors using hydrometallurgical routes, J. Environ. Chem. Eng. 10 (2022) 108182, https://doi.org/10.1016/J.JECE.2022.108182.
[28] M. Agrawal, K.K. Singh, R. Singh, Hydrometallurgical recovery of manganese and nickel and isolation of tantalum from obsolete tantalum capacitor, J. Environ. Chem. Eng. 10 (2022) 108887, https://doi.org/10.1016/J.JECE.2022.108887.
[29] D. Wang, Q. Li, X. Guo, X. Zou, Study on dissolution mechanism of mineral/liquid interface during HF acid leaching niobium-tantalum ore, Miner. Eng. 188 (2022) 107835, https://doi.org/10.1016/J.MINENG.2022.107835.
[30] O.M. El-Hussaini, M.A. Mahdy, Sulfuric acid leaching of Kab Amiri niobium–tantalum bearing minerals, central Eastern Desert, Egypt, Hydrometallurgy 64 (2002) 219–229, https://doi.org/10.1016/S0304-386X(02)00045-2.
[31] B. Wu, H. Shang, J.-K. Wen, Sulfuric acid leaching of low-grade refractory tantalum–niobium and associated rare earths minerals in Panxi area of China, Rare Metals 34 (2015) 202–206, https://doi.org/10.1007/s12598-014-0436-7.
[32] M. Moradi, A.M. Ferreira, C.M.S.S. Neves, F.H.B. Sosa, G. Pazuki, J.A.P. Coutinho, Enantioseparation of ofloxacin using a liquid–liquid extraction system based on hydrophobic eutectic solvents, Sep. Purif. Technol. 353 (2025) 128462, https://doi.org/10.1016/j.seppur.2024.128462.
[33] N. Begum, F. Bari, S.B. Jamaludin, K. Hussin, Solvent extraction of copper, nickel and zinc by Cyanex 272, Int. J. Phys. Sci. 7 (2012) 2905–2910, https://doi.org/10.5897/IJPS12.116.
[34] L. Velásquez-Yévenes, R. Ram, The aqueous chemistry of the copper-ammonia system and its implications for the sustainable recovery of copper, Cleaner Eng. Technol. 9 (2022) 100515, https://doi.org/10.1016/J.CLET.2022.100515.
[35] V. Innocenzi, F. Veglio, Separation of manganese, zinc and nickel from leaching solution of nickel-metal hydride spent batteries by solvent extraction, Hydrometallurgy 129–130 (2012) 50–58, https://doi.org/10.1016/j.hydromet.2012.08.003.
[36] ISO, ISO 14040. Environmental management – Life cycle assessment – Principles and framework, Geneva, Switzerland, 2006.
[37] ISO, ISO 14044. Environmental management - Life cycle assessment – Requirements and guidelines, Geneva, Switzerland, 2006.
[38] M. Rinne, R. Aromaa-Stubb, H. Elomaa, A. Porvali, M. Lundström, Evaluation of hydrometallurgical black mass recycling with simulation-based life cycle assessment, Int. J. Life Cycle Assess. 29 (2024) 1582–1597, https://doi.org/10.1007/s11367-024-02304-y.
[39] D.W. Fuerstenau, A.Z. Abouzeid, The energy efficiency of ball milling in comminution, Int. J. Miner. Process. 67 (2002) 161–185, https://doi.org/10.1016/S0301-7516(02)00039-X.
[40] R.K. Sinnott, Equipment selection, specification and design, in: Coulson and Richardson's Chemical Engineering, Pergamon, 1993, pp. 352–438, https://doi.org/10.1016/B978-0-08-041865-0.50018-0.
[41] M. Huttunen, L. Nygren, T. Kinnarinen, A. Häkkinen, T. Lindh, J. Ahola, V. Karvonen, Specific energy consumption of cake dewatering with vacuum filters, Miner. Eng. 100 (2017) 144–154, https://doi.org/10.1016/J.MINENG.2016.10.025.
[42] G. Wernet, C. Bauer, B. Steubing, J. Reinhard, E. Moreno-Ruiz, B. Weidema, The ecoinvent database version 3 (part I): overview and methodology, Int. J. Life Cycle Assess. 21 (2016) 1218–1230, https://doi.org/10.1007/s11367-016-1087-8.
[43] S. Andreasi Bassi, F. Biganzoli, N. Ferrara, A. Amadei, A. Valente, S. Sala, F. Ardente, Updated characterisation and normalisation factors for the environmental footprint 3.1 method, 2023, https://doi.org/10.2760/798894.
[44] A. Ashiq, J. Kulkarni, M. Vithanage, Hydrometallurgical recovery of metals from E-waste, in: M.N.V. Prasad, M. Vithanage (Eds.), Electronic Waste Management and Treatment Technology, Butterworth-Heinemann, 2019, pp. 225–246, https://doi.org/10.1016/B978-0-12-816190-6.00010-8.
[45] D.R. Lide (Ed.), CRC Handbook of Chemistry and Physics, CRC Press, Boca Raton, 2005.
[46] M.H. Lietzke, R.W. Stoughton, The solubility of silver sulfate in sulfuric acid Media at High Temperatures. Effects on the silver, silver sulfate electrode, J. Am. Chem. Soc. 78 (1956) 3023–3025, https://doi.org/10.1021/ja01594a024.
[47] J. Partinen, P. Halli, B.P. Wilson, M. Lundström, The impact of chlorides on NMC leaching in hydrometallurgical battery recycling, Miner. Eng. 202 (2023) 108244, https://doi.org/10.1016/J.MINENG.2023.108244.
[48] G.P. Zaraisky, V. Korzhinskaya, N. Kotova, Experimental studies of Ta2O5 and columbite–tantalite solubility in fluoride solutions from 300 to 550 °C and 50 to 100 MPa, Mineral. Petrol. 99 (2010) 287–300, https://doi.org/10.1007/s00710-010-0112-z.
[49] F. Fairbrother, J.B. Taylor, Water-soluble complexes of niobium (columbium) and tantalum. Part I. Complexes with α-hydroxy-acids and (2-hydroxyethyl)-amines, J. Chem. Soc. 0 (1956) 4946–4954, https://doi.org/10.1039/JR9560004946.
[50] A. Shikika, M. Sethurajan, F. Muvundja, M.C. Mugumaoderha, S. Gaydardzhiev, A review on extractive metallurgy of tantalum and niobium, Hydrometallurgy 198 (2020) 105496, https://doi.org/10.1016/J.HYDROMET.2020.105496.
[51] A.B. Botelho Junior, D.C.R. Espinosa, J. Vaughan, J.A.S. Tenório, Recovery of scandium from various sources: a critical review of the state of the art and future prospects, Miner. Eng. 172 (2021) 107148, https://doi.org/10.1016/J.MINENG.2021.107148.
[52] L. Kong, Z. Wang, Z. Shi, X. Hu, A. Liu, W. Tao, B. Wang, Q. Wang, Leaching valuable metals from spent lithium-ion batteries using the reducing agent methanol, Environ. Sci. Pollut. Res. 30 (2023) 4258–4268, https://doi.org/10.1007/s11356-022-22414-0.
[53] K.C. Liddell, Shrinking core models in hydrometallurgy: what students are not being told about the pseudo-steady approximation, Hydrometallurgy 79 (2005) 62–68, https://doi.org/10.1016/J.HYDROMET.2003.07.011.
[54] O. Levenspiel, Chapter 25 - fluid-particle reactions: Kinetics, in: Chemical Reaction Engineering, 3rd ed., John Wiley & Sons, New York, NY, 1999, pp. 566–588.
[55] M. Bugarčić, A. Jovanović, D. Anđić, I. Jelić, M. Miletić, B. Marković, M. Sokić, Kinetics of sphalerite leaching by MnO2-KI oxidation system in sulfuric acid, Metals (Basel). 15 (2025) 50, https://doi.org/10.3390/met15010050.
[56] W. Xiao, X. Liu, Z. Zhao, Kinetics of nickel leaching from low-nickel matte in sulfuric acid solution under atmospheric pressure, Hydrometallurgy 194 (2020) 105353, https://doi.org/10.1016/J.HYDROMET.2020.105353.
[57] M.C. Ruiz, R. Padilla, Copper removal from molybdenite concentrate by sodium dichromate leaching, Hydrometallurgy 48 (1998) 313–325, https://doi.org/10.1016/S0304-386X(98)00006-1.
[58] E.A. Abdel-Aal, Kinetics of sulfuric acid leaching of low-grade zinc silicate ore, Hydrometallurgy 55 (2000) 247–254, https://doi.org/10.1016/S0304-386X(00)00059-1.
[59] J. Sun, T. Zhang, P. Shen, D. Liu, L. Dong, Kinetics analysis of copper extraction from copper smelting slag by sulfuric acid oxidation leaching, Miner. Eng. 216 (2024) 108886, https://doi.org/10.1016/J.MINENG.2024.108886.
[60] Y. Kim, J. Lee, Leaching kinetics of zinc from metal oxide Varistors (MOVs) with sulfuric acid, Metals (Basel). 6 (2016) 192, https://doi.org/10.3390/met6080192.
[61] C. Özmetin, M. Çopur, A. Yartasi, M.M. Kocakerim, Kinetic investigation of reaction between metallic silver and nitric acid solutions, Chem. Eng. Technol. 23 (2000) 707–711, https://doi.org/10.1002/1521-4125(200008)23:8<707::AID-CEAT707>3.0.CO;2-L.
[62] C. Özmetin, M. Çopur, A. Yartasi, M. Muhtar Kocakerim, Kinetic investigation of reaction between metallic silver and nitric acid solutions in the range 7.22−14.44 M, Ind. Eng. Chem. Res. 37 (1998) 4641–4645, https://doi.org/10.1021/ie980121w.
[63] S. Aktas, Silver recovery from spent silver oxide button cells, Hydrometallurgy 104 (2010) 106–111, https://doi.org/10.1016/J.HYDROMET.2010.05.004.
[64] E. Allain, N. Kanari, F. Diot, J. Yvon, Development of a process for the concentration of the strategic tantalum and niobium oxides from tin slags, Miner. Eng. 134 (2019) 97–103, https://doi.org/10.1016/J.MINENG.2019.01.029.
[65] D.K. Rajak, R. Jordaan, A. Gómez-Arias, W. Purcell, Extractive metallurgy of columbite-tantalite ore: a detailed review, Miner. Eng. 190 (2022) 107917, https://doi.org/10.1016/J.MINENG.2022.107917.

[66] R.M. Freitas, T.A.G. Perilli, A.C.Q. Ladeira, Oxidative precipitation of manganese from acid mine drainage by potassium permanganate, J. Chem. (2013) 1220, https://doi.org/10.1155/2013/287257.
[67] D.S. Flett, Solvent extraction in hydrometallurgy: the role of organophosphorus extractants, J. Organomet. Chem. 690 (2005) 2426–2438, https://doi.org/10.1016/J.JORGANCHEM.2004.11.037.
[68] X. Meng, K.N. Han, The principles and applications of Ammonia leaching of metals—a review, Miner. Process. Extr. Metall. Rev. 16 (1996) 23–61, https://doi.org/10.1080/08827509608914128.
[69] A.M.I. Ali, I.M. Ahmad, J.A. Daoud, CYANEX 272 for the extraction and recovery of zinc from aqueous waste solution using a mixer-settler unit, Sep. Purif. Technol. 47 (2006) 135–140, https://doi.org/10.1016/J.SEPPUR.2005.06.015.
[70] W. Liu, J. Zhang, Z. Xu, J. Liang, Z. Zhu, Study on the extraction and separation of zinc, cobalt, and nickel using Ionquest 801, Cyanex 272, and their mixtures, Metals (Basel). 11 (2021) 401, https://doi.org/10.3390/met11030401.
[71] K. Binnemans, P.T. Jones, Methanesulfonic acid (MSA) in hydrometallurgy, Journal of Sustainable Metallurgy 9 (2023) 26–45, https://doi.org/10.1007/s40831-022-00641-6.
[72] W.M. Haynes, D.R. Lide, T.J. Bruno, CRC Handbook of Chemistry and Physics, 97th ed., CRC Press, Boca Raton, 2005.